

Supplementary Material

A comprehensive kinetic modeling of oxymethylene ethers (OMEn, n=1-3) oxidation - laminar flame speed and ignition delay time measurements

Krishna P. Shrestha^{a,*}, Sven Eckart^b, Simon Drost^c, Chris Fritzsche^b, Robert Schießl^c, Lars Seidel^d, Ulrich Maas^c, Hartmut Krause^b, Fabian Mauss^a

^a *Thermodynamics and Thermal Process Engineering, Brandenburg University of Technology, Siemens-Halske-Ring 8, 03046 Cottbus, Germany*

^b *Institute of Thermal Engineering, TU Bergakademie Freiberg, Freiberg, Germany*

^c *Karlsruhe Institute of Technology, Institute of Technical Thermodynamics, Engelbert-Arndold-Strasse 4, 76131 Karlsruhe, Germany*

^d *LOGE Deutschland GmbH, Querstraße 48, 03044 Cottbus, Germany*

*Corresponding author: shrestha@b-tu.de

<https://doi.org/10.1016/j.combustflame.2022.112426>

The present model also contains NH₃ and NO_x mechanism which can be used for investigating NH₃ and NO_x as well as its blend with other fuels.

Please see the mechanism file which list the fuels for which the mechanism has been validated.

Table S 1: List of updated and/or added new reactions in OME₂ and OME₃ sub-mechanism compared to He et al. [1] model.

Reactions	Source of rate constant
OME ₂ (+M) => CH ₃ OH + HCO + CH ₃ OCH ₂ (+M)	Zhong et al. [2]
OME ₂ (+M) => CH ₃ OCH ₂ OH + HCO + CH ₃ (+M)	Zhong et al. [2]
OME ₂ (+M) = CH ₃ OCH ₂ OCH ₂ + CH ₃ O(+M)	est. DEM = C ₂ H ₅ OCH ₂ + C ₂ H ₅ O Zhang et al. [3]
OME ₂ (+M) = CH ₃ OCH ₂ O + CH ₃ OCH ₂ (+M)	est. DEM = C ₂ H ₅ OCH ₂ O + C ₂ H ₅ Zhang et al. [3]
OME ₂ + CH ₃ O ₂ = OME ₂ A + CH ₃ O ₂ H	est. DMM + CH ₃ O ₂ Shrestha et al. [4]
OME ₂ + CH ₃ O ₂ = OME ₂ B + CH ₃ O ₂ H	est. DMM + CH ₃ O ₂ Shrestha et al. [4]
OME ₂ + CH ₃ O = OME ₂ A + CH ₃ OH	Cai et al. [5]
OME ₂ + CH ₃ O = OME ₂ B + CH ₃ OH	Cai et al. [5]
OME ₂ + CH ₃ = OME ₂ A + CH ₄	Cai et al. [5]
OME ₂ + CH ₃ = OME ₂ B + CH ₄	Cai et al. [5]
OME ₂ + HO ₂ = OME ₂ A + H ₂ O ₂	Cai et al. [5]
OME ₂ + HO ₂ = OME ₂ B + H ₂ O ₂	Cai et al. [5]
OME ₃ (+M) = CH ₃ OCH ₂ OCH ₃ + CH ₃ OCHO(+M)	Zhong et al. [2]
OME ₃ (+M) => CH ₃ OCH ₂ OH + HCO + CH ₃ OCH ₂ (+M)	Zhong et al. [2]
OME ₃ (+M) => CH ₃ OH + HCO + CH ₃ OCH ₂ OCH ₂ (+M)	Zhong et al. [2]
OME ₃ (+M) => CH ₃ OCH ₂ OCH ₂ OH + HCO + CH ₃ (+M)	Zhong et al. [2]
OME ₃ (+M) = OME ₂ A + CH ₃ O(+M)	est. DEM = C ₂ H ₅ OCH ₂ + C ₂ H ₅ O Zhang et al. [3]
OME ₃ (+M) = CH ₃ OCH ₂ OCH ₂ O + CH ₃ OCH ₂ (+M)	est. DEM = C ₂ H ₅ OCH ₂ O + C ₂ H ₅ Zhang et al. [3]
OME ₃ =OME ₃ A+H	Cai et al. [5]
OME ₃ =OME ₃ B+H	Cai et al. [5]
OME ₃ =OME ₃ C+H	Cai et al. [5]
OME ₃ + CH ₃ O =OME ₃ A+CH ₃ OH	Cai et al. [5]
OME ₃ + CH ₃ O =OME ₃ B+CH ₃ OH	Cai et al. [5]
OME ₃ + CH ₃ O =OME ₃ C+CH ₃ OH	Cai et al. [5]
CH ₃ OCH ₂ OH(+M) = CH ₃ OH + CH ₂ O(+M)	Zhong et al. [2]
CH ₃ OCH ₂ OH = CH ₃ O + CH ₂ OH	Zhong et al. [2]
CH ₃ OCH ₂ OH = CH ₃ OCH ₂ + OH	Zhong et al. [2]
CH ₃ OCH ₂ OCH ₂ OH = CH ₃ O + CH ₂ OCH ₂ OH	Zhong et al. [2]
CH ₃ OCH ₂ OCH ₂ OH = CH ₃ OCH ₂ O + CH ₂ OH	Zhong et al. [2]
CH ₃ OCH ₂ OCH ₂ OH = CH ₂ O + CH ₃ OCH ₂ OH	Zhong et al. [2]
CH ₃ OCH ₂ OCH ₂ OH = CH ₃ OCHO + CH ₃ OH	Zhong et al. [2]
C ₂ H ₅ + HO ₂ = C ₂ H ₄ + H ₂ O ₂	Ludwig et al. [6]
C ₂ H ₅ + HO ₂ = C ₂ H ₅ O + OH	Ludwig et al. [6]

Table S 2: List of kinetic models used for comparison against the present and literature experimental data. For experimental conditions follow the case number as shown in the Table 2 in main manuscript. Three model are chosen for comparison: Cai et al. [5], He et al. [1] and Ras et al. [7]. S is the Figure number means that the figure is in supplementary material if not it is in the main manuscript.

Case	This model	Cai 2020 model	He 2018 model	Ras 2022 model	Displayed in
OME₂					
1	☒	☒			Figure 5, Figure S 5 , Figure S 7
2	☒				Figure S 9
3	☒	☒	-	-	Figure S 10
4	☒				Figure S 18
5	☒	☒	☒	☒	Figure 11, Figure S 13 , Figure S 15
6	☒	☒	☒	☒	Figure 10
7	-	-	-	-	
8	☒	☒	☒		Figure 10, Figure S 12
9	☒	☒	☒	☒	Figure 15, Figure S 26 , Figure S 27
10	☒	-	-	-	Figure S 4
12	☒	-	-	-	Figure S 31
13	☒	☒	☒	☒	Figure 2, Figure S 2
OME₃					
14	☒	☒			Figure 6, Figure S 5 , Figure S 7
15	☒	☒	-	-	Figure 6
16	☒				Figure S 11
17	☒	☒	☒		Figure 12, Figure S 13 , Figure S 16
18	☒	☒	☒		Figure 11
19	☒	☒	☒		Figure 11, Figure S 12
20	☒	☒	☒		Figure 11, Figure S 12
21	-	-	-	-	
22	☒	☒	☒		Figure S 28 , Figure S 29 , Figure S 30
23	☒	☒	☒		Figure 16, Figure S 21 , Figure S 22 , Figure S 23 , Figure S 24 , Figure S 25
24	☒	☒	☒		Figure 2, Figure S 3
25	☒				Figure S 33
26	☒				Figure S 32

Table S 3: Experimental data and measurement ,uncertainty for OME₁, OME₂ and OME₃ at 1-5 bar at temperature 393-443K. S_L: Laminar flame speed, ΔS_L: uncertainty in measurmemt.

OME ₁	1bar - 443K		3bar - 443K			
	φ	S _L [cm/s]	ΔS _L [cm/s]	φ	S _L [cm/s]	ΔS _L [cm/s]
0.80	64.00	0.37		0.80	48.38	0.25
0.90	70.27	1.11		0.90	55.12	1.66
1.00	81.67	2.07		1.00	63.90	1.43
1.10	85.00	1.30		1.10	67.40	0.22
1.20	82.98	0.52		1.20	66.10	0.23
1.30	78.55	0.42		1.30	59.87	0.21
1.40	77.63	1.18		1.40	57.23	0.84

OME ₂	3bar - 393K		5bar - 393K		1bar - 443K		3bar - 443K		
	φ	S _L [cm/s]	ΔS _L [cm/s]	φ	S _L [cm/s]	ΔS _L [cm/s]	φ	S _L [cm/s]	ΔS _L [cm/s]
0.80	43.22	0.33		35.60	0.25		67.73	8.26	48.67
0.90	51.00	0.24		42.80	0.71		79.70	1.56	60.35
1.00	57.08	0.26		48.87	0.25		83.10	1.61	65.84
1.10	59.22	1.36		53.60	0.28		87.18	1.89	71.02
1.20	56.92	2.59					91.36	1.83	71.28
1.30	54.23	3.37					86.42	2.16	66.97
1.40	48.08	1.38					73.63	4.85	55.32
									3.76

OME ₃	1bar - 443K		3bar - 443K			
	φ	S _L [cm/s]	ΔS _L [cm/s]	φ	S _L [cm/s]	ΔS _L [cm/s]
0.80	57.17	1.72		0.80	40.80	6.20
0.90	73.50	1.01		0.90	56.00	1.14
1.00	85.03	1.00		1.00	59.52	0.36
1.10	97.27	1.27		1.10	65.20	1.79
1.20	96.13	0.12		1.20	71.88	0.31
1.30	91.63	0.97				
1.40	82.63	3.94				
1.50	68.93	2.67				
1.60	67.30	0.57				

Table S 4: Calculated Markstein length for OME₁, OME₂ and OME₃ at 443K and 1 bar.

	OME₁	OME₂	OME₃
ϕ	L_b	L_b	L_b
0.8	0.170072	0.158959	0.142449
0.9	0.154263	0.128293	0.114526
1.0	0.102564	0.110021	0.133647
1.1	0.074048	0.095158	
1.2	0.055966	0.056031	0.101327
1.3	0.025292	0.044234	
1.4	0.012764	-0.01706	0.05029
1.6			-0.0012

1. Pyrolysis - OME₁, OME₂, and OME₃

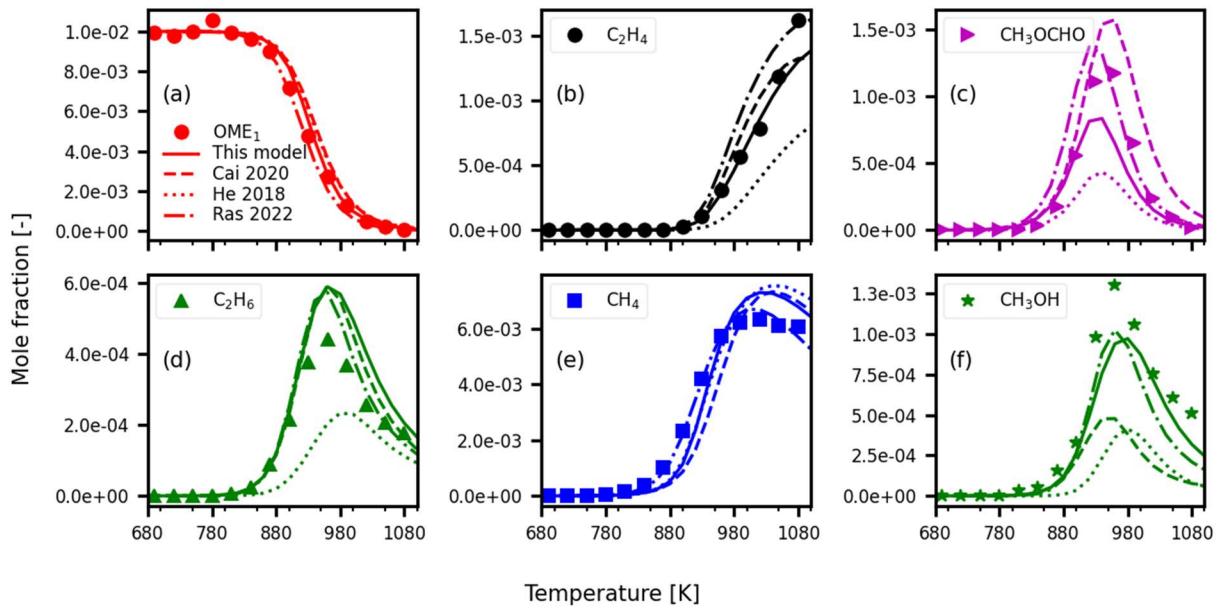


Figure S 1: OME₁/Ar pyrolysis in a jet-stirred reactor 1 atm, $\tau = 2$ s. Symbols: experimental data from Zhong et al. [2], solid lines: this model, dashed lines: Cai model [5], dotted lines: He model [1], dashed-dot lines: Ras model [7].

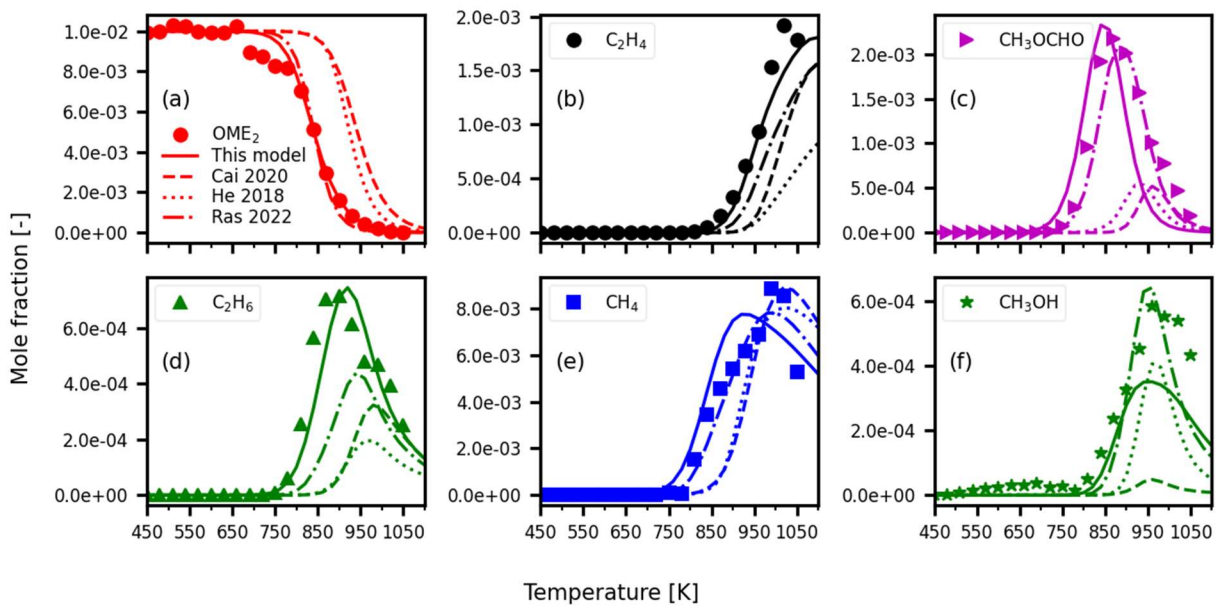


Figure S 2: OME_2/Ar pyrolysis in a jet-stirred reactor 1 atm, $\tau = 2$ s. Symbols: experimental data from Zhong et al. [2], solid lines: this model, dashed lines: Cai model [5], dotted lines: He model [1], dashed-dot lines: Ras model [7].

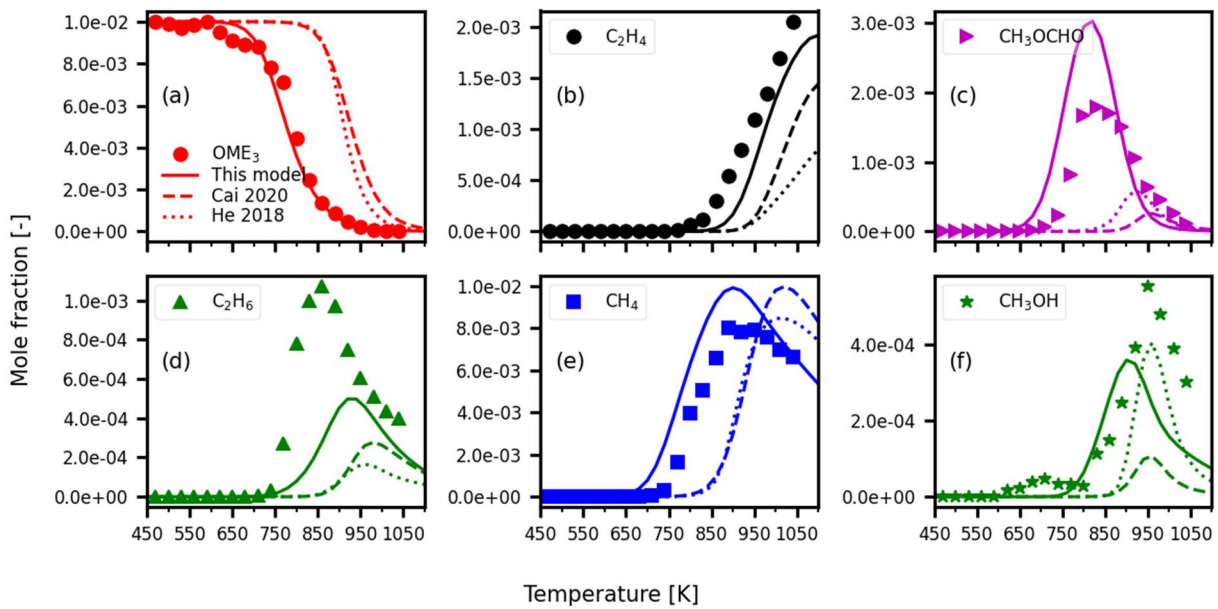


Figure S 3: OME_3/Ar pyrolysis in a jet-stirred reactor 1 atm, $\tau = 2$ s. Symbols: experimental data from Zhong et al. [2], solid lines: this model, dashed lines: Cai model [5], dotted lines: He model [1].

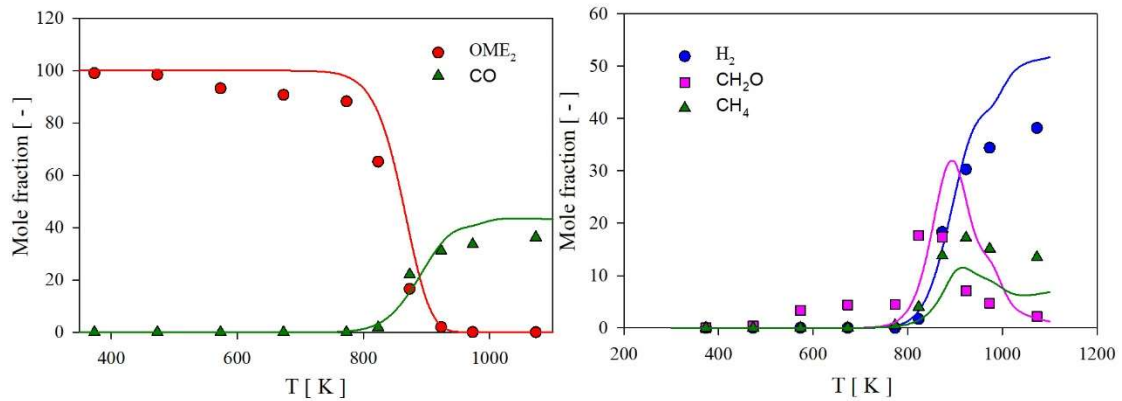


Figure S 4: Pyrolysis of OME₂/He in a plug flow reactor. Symbols: experimental data from De Ras et al. [7], lines: model predictions from this work.

2. Laminar flame speed - OME₁, OME₂, and OME₃

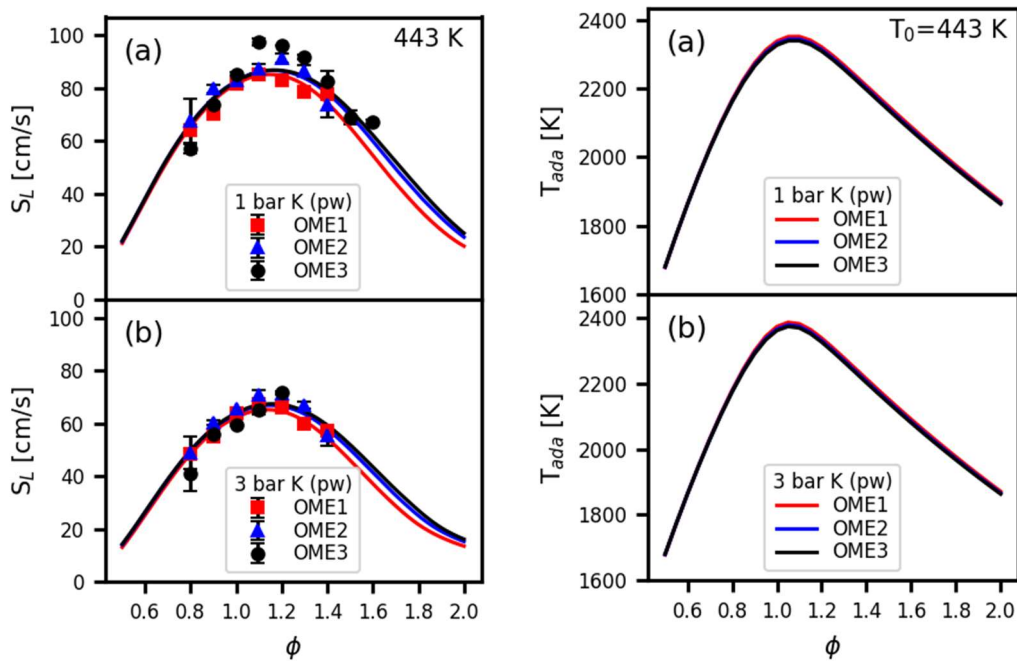


Figure S 5: Symbols: experimental data from present work, lines: this model predictions. left: laminar flame speed, right: adiabatic flame temperature.

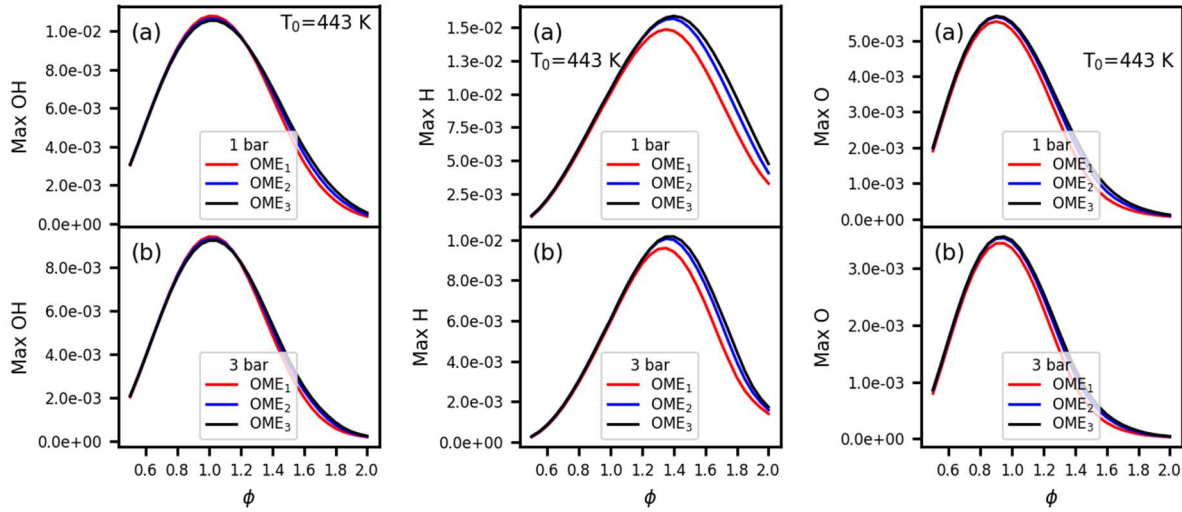


Figure S 6: This model predicted species profile of OH (left), H (center) and O (right) of OME₁, OME₂, and OME₃ flames.

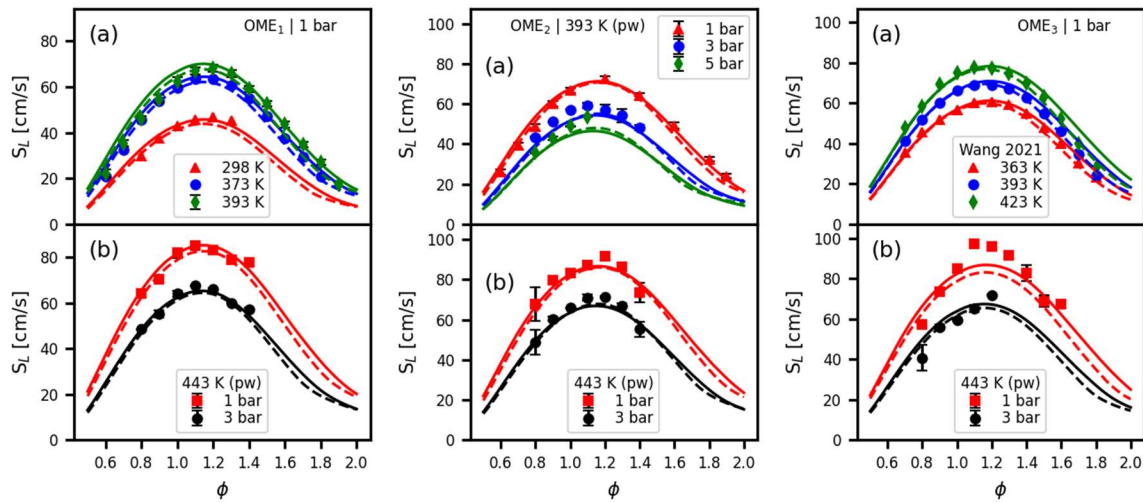


Figure S 7: Laminar burning velocity of OME₁/air (left), OME₂/air (center,) and OME₃/air (right). Symbols: present experimental data and from literature (OME₁/air 1 bar [4,8] and OME₃/air 1 bar [9]). Solid lines: this model predictions, dashed lines: Sun et al. [10] model predictions.

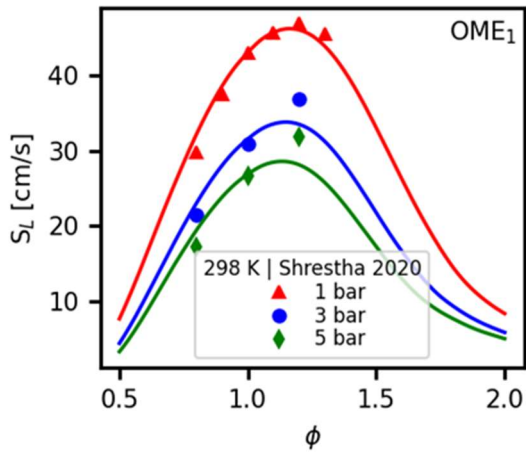


Figure S 8: Laminar flame speed of OME_1 /air at 298 K and different pressure. Symbols: experimental data from Shrestha et al. [4], lines: model predictions from this work.

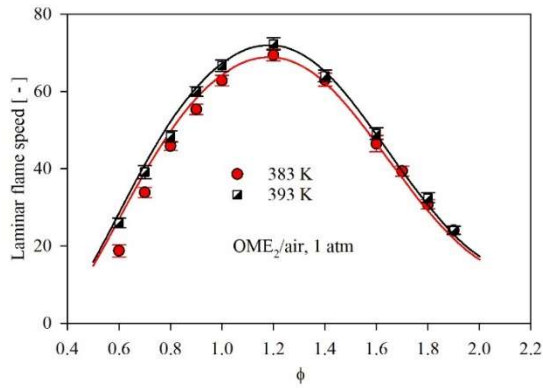


Figure S 9: Laminar flame speed of OME_2 /air at 1 atm and different temperatures. Symbols: experiments from Eckart et al. [8], lines: model predictions from this work.

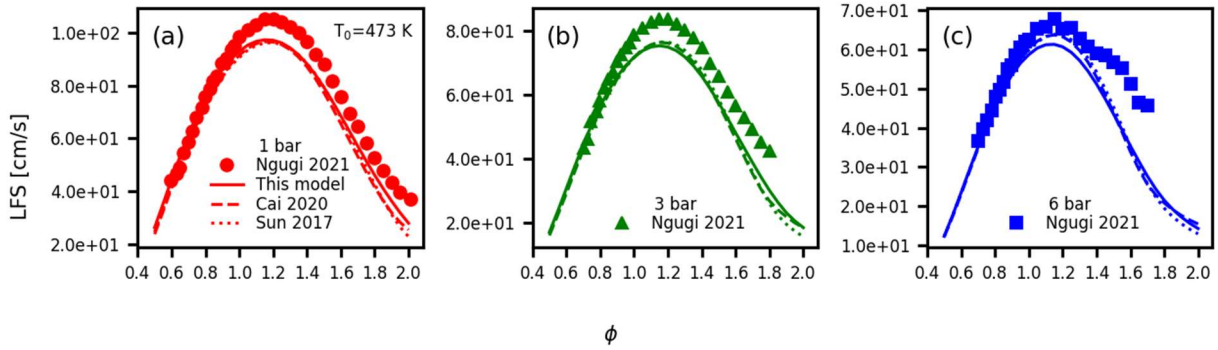


Figure S 10: Laminar flame speed of OME_2/air at 473 K and different pressure. Symbols: experiments from Ngugi et al. [11], lines: model predictions; solid lines: this work, dashed lines: Cai model [5], dotted lines: Sun model [10]

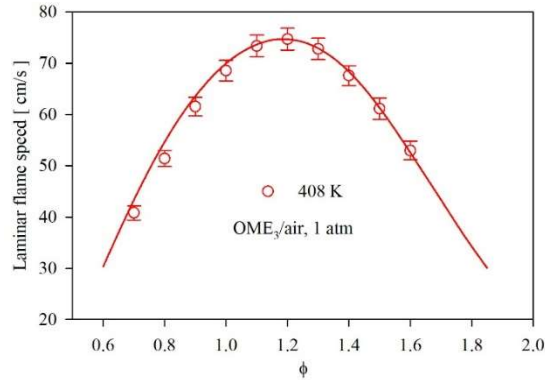


Figure S 11: Laminar flame speed of OME_3/air at 1 atm and 408 K. Symbols: experiments from Sun et al. [10], lines: model predictions from this work.

3. Ignition delay time - OME₁, OME₂, and OME₃

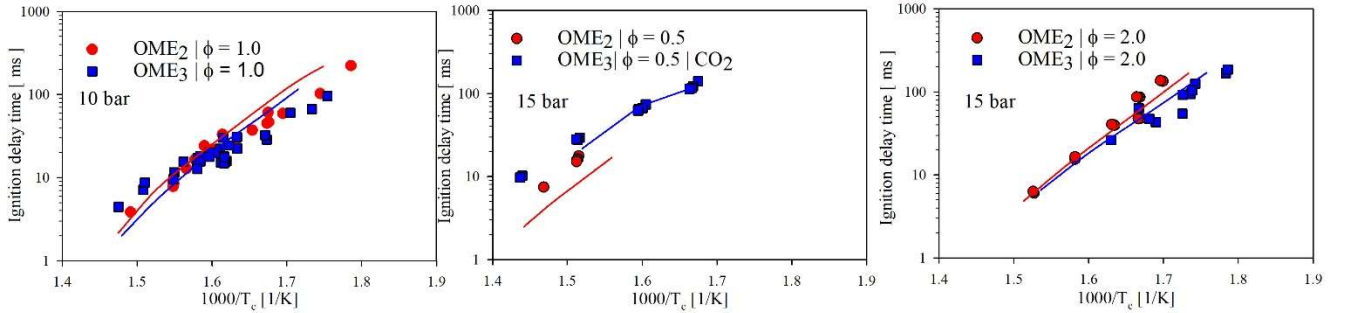


Figure S 12: Ignition delay time comparison of OME₂ and OME₃. Symbols: measurement, $\phi = 1.0$ and 10 bar from [12], $\phi = 0.5$ and 2.0 (present work). Lines: this model predictions.

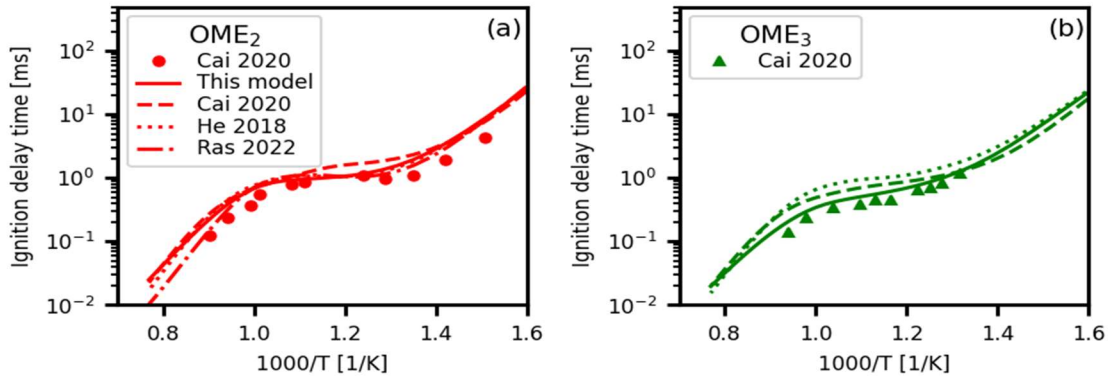


Figure S 13: Ignition delay time of OME₂ and OME₃ at 10 bar, $\phi = 1.0$. Symbols: shock tube experiments from Cai et. al. [5]. Solid lines: this model, dashed lines: Cai [5], dotted: He [1], dashed-dotted: Ras [7].

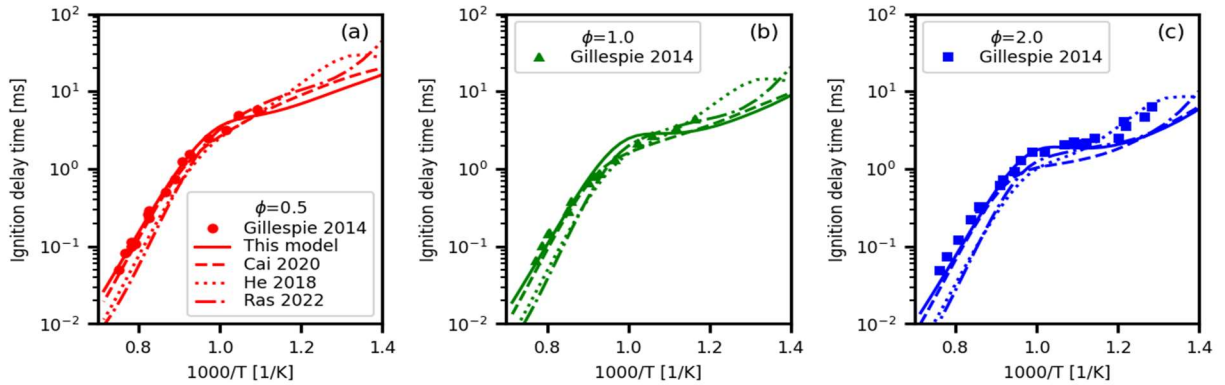


Figure S 14: Ignition delay time of $\text{OME}_1/\text{O}_2/\text{N}_2$ at 10 bar and different equivalence ratio. Symbols: experiments from Gillespie [13], solid lines: this model, dashed lines: Cai model [5], dotted lines: He model [1], dashed-dotted lines: Ras model [7].

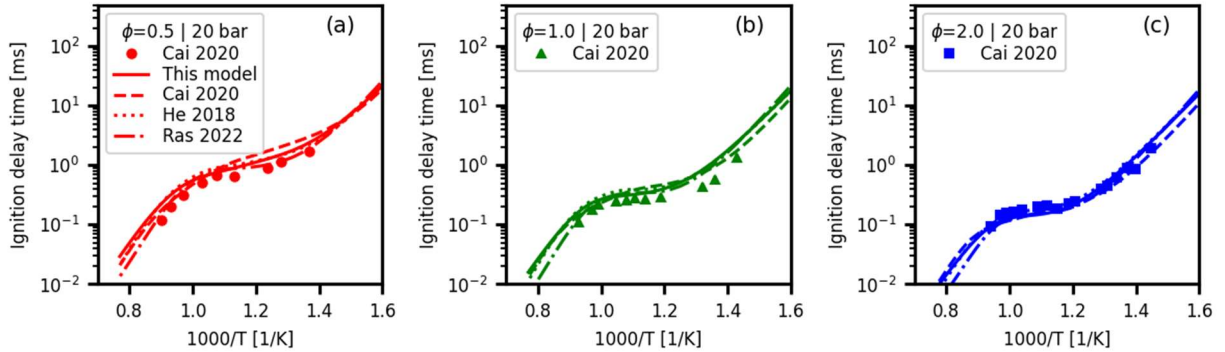


Figure S 15: Ignition delay time of $\text{OME}_2/\text{O}_2/\text{N}_2$ at $\phi = 0.5-2.0$ and 20 bar. Symbols: experiments from Cai et al. [5], solid lines: this model, dashed lines: Cai model [5], dotted lines: He model [1], dashed-dotted lines: Ras model [7].

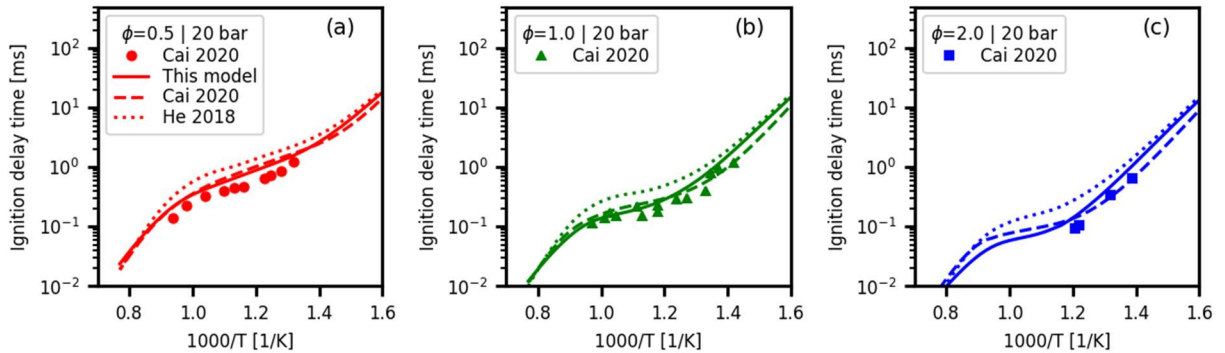


Figure S 16: Ignition delay time of OME_3/air at 20 bar, $\phi = 0.5-2.0$. Symbols: experiments from Cai et al. [5], solid lines: this model, dashed lines: Cai model [5], dotted lines: He model [1].

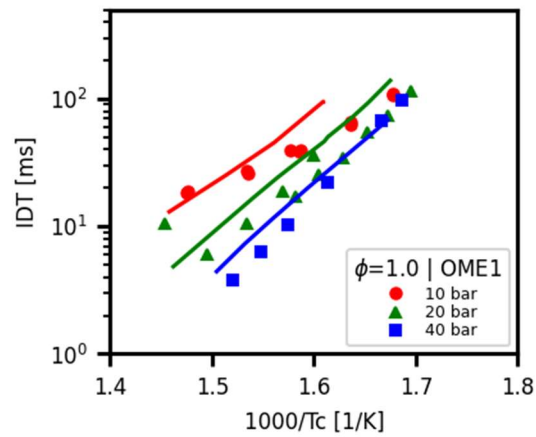


Figure S 17: Ignition delay time (RCM) of $\text{OME}_1/\text{O}_2/\text{N}_2$ at $\phi=1.0$, 10-40 bar. Symbols: experiments from Gillespie [13], lines: model predictions from this work.

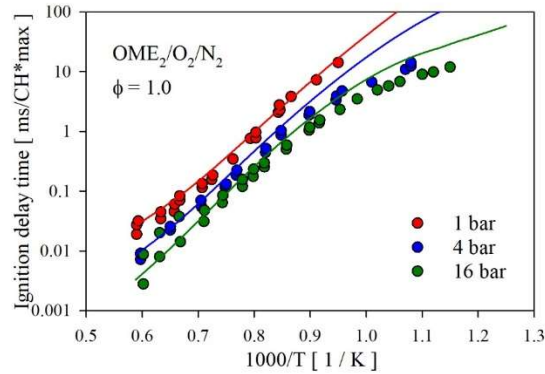


Figure S 18: Ignition delay time of $\text{OME}_2/\text{O}_2/\text{N}_2$ at different pressure. Symbols: experiments from Ngugi et al. [11], lines: model predictions from this work.

4. Speciation in jet-stirred reactor - OME₁, OME₂, and OME₃

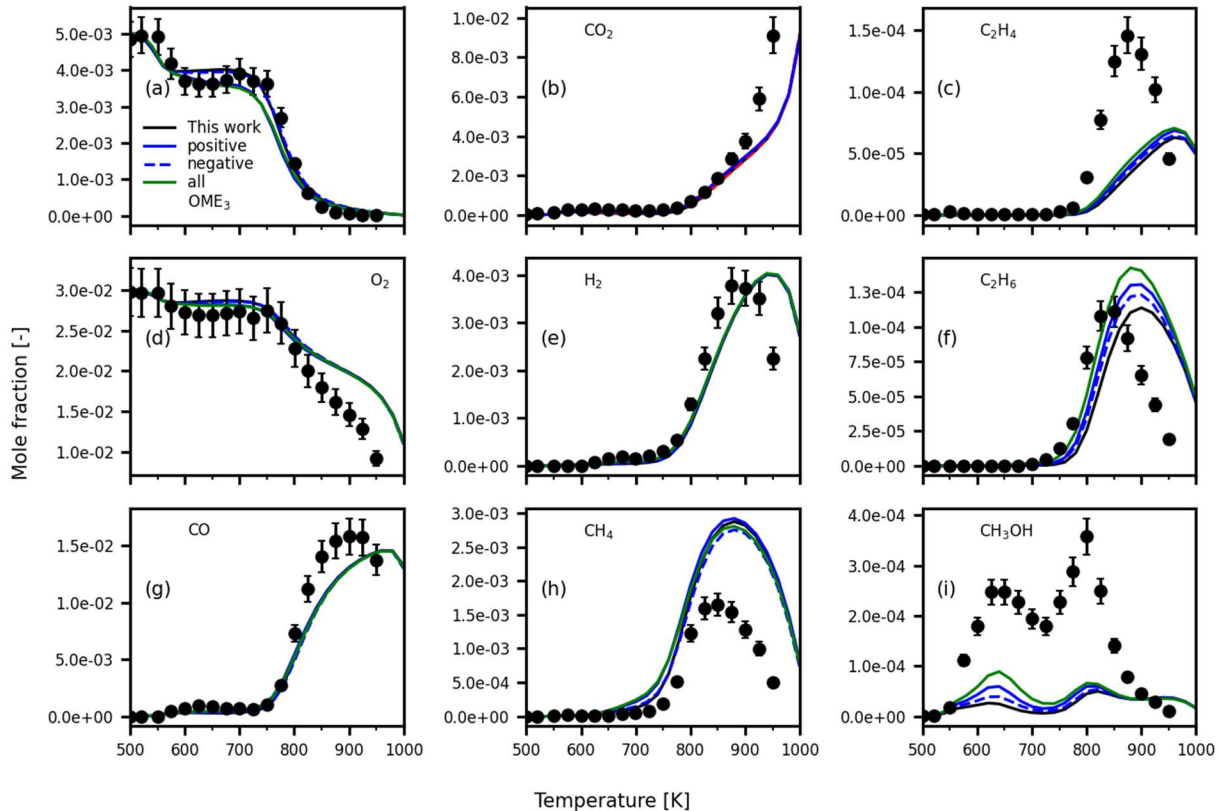


Figure S 19: Comparison of the model predictions against the experimental data (shown in Figure 16) by changing the rate coefficient listed in Figure 17 (sensitivity analysis) by 50%. Positive increasing the rate coefficients of reactions showing positive sensitivity in Figure 17. Negative: decreasing the rate coefficients of reactions showing negative sensitivity in Figure 17. All: This work both positive and negative sensitivity changes implemented simultaneously as shown in Figure 17. This work: without any changes (model proposed in this work).

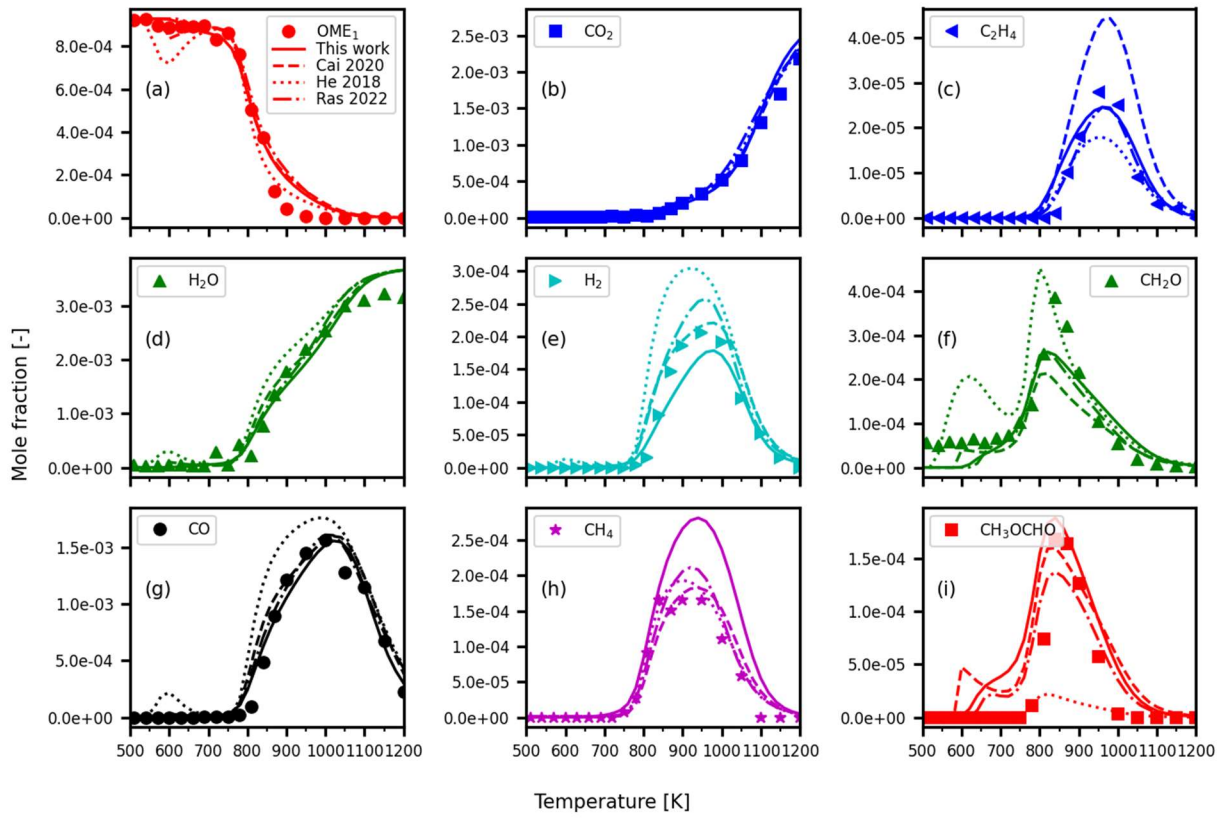


Figure S 20: OME₁/O₂/N₂ oxidation in jet-stirred reactor at $\phi = 0.5$, 10 atm, $\tau = 0.7$ s. Symbols: experimental data from Sun et al. [14], solid lines: this model, dashed lines: Cai model [5], dotted lines: He model [1], dashed-dot lines: Ras model [7].

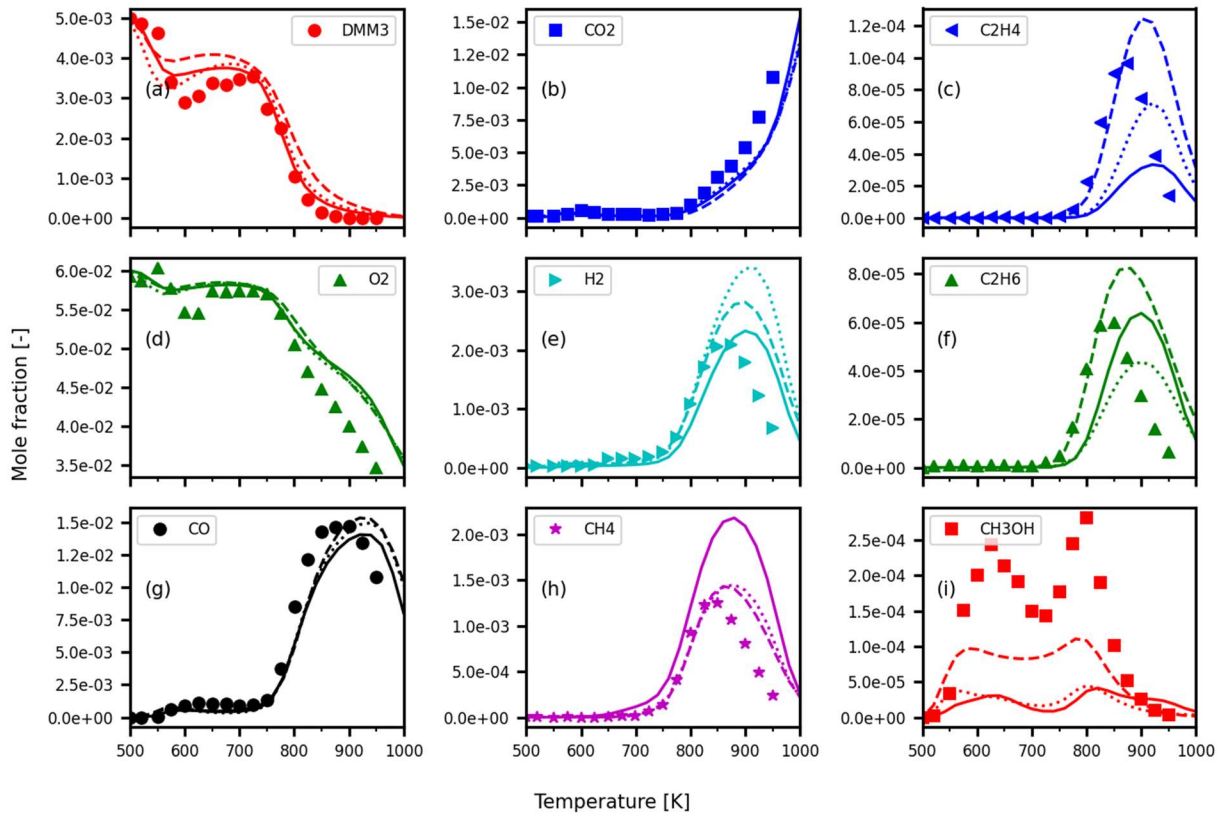


Figure S 21: Oxidation of $\text{OME}_3/\text{O}_2/\text{N}_2$ in a jet-stirred reactor at $\phi = 0.5$, 1 atm and $\tau = 2$ s. Symbols: experimental data from Qiu et al. [15], solid lines: this model, dashed lines: Cai model [5], dotted lines: He model [1]. DMM3: OME_3 .

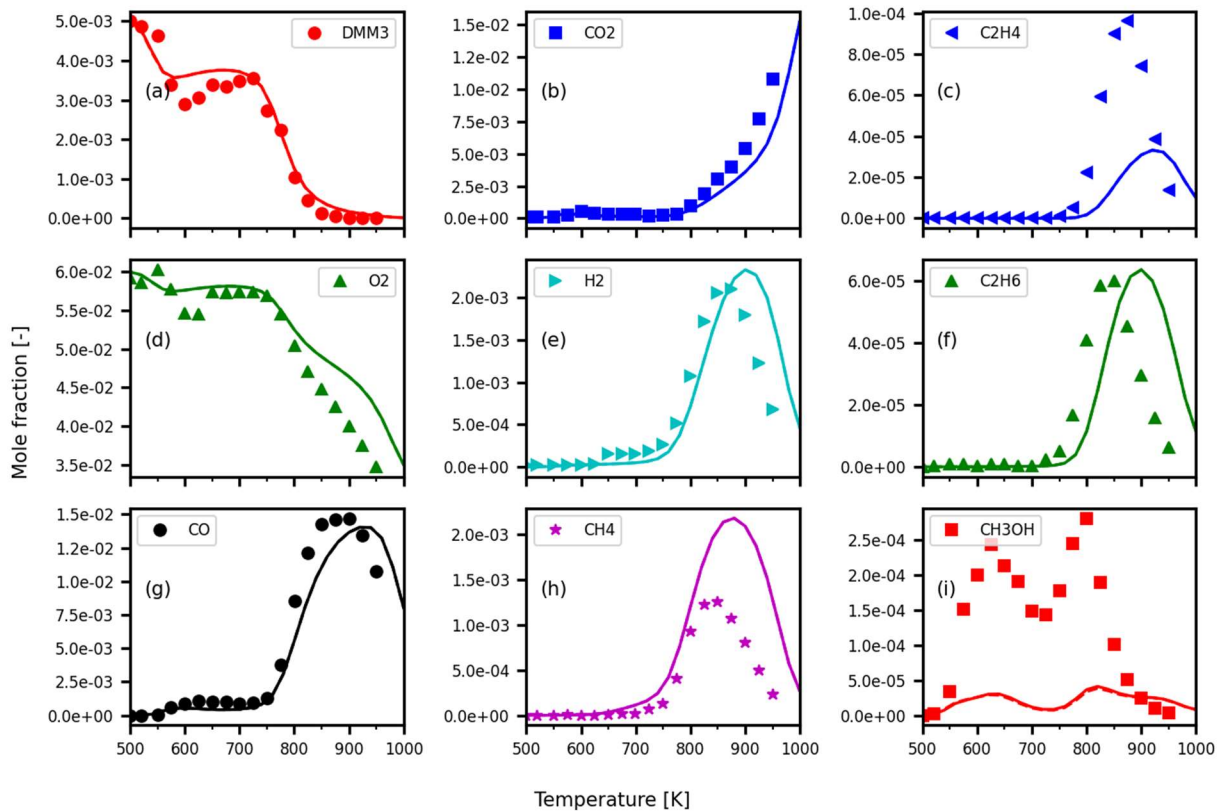


Figure S 22: Oxidation of OME₃/O₂/N₂ in a jet-stirred reactor at $\phi = 0.5$, 1 atm and $\tau = 2$ s. Symbols: experimental data from Qiu et al. [15], solid lines: this model, dashed lines: implementing OME₃ + CH₃O reaction rate from Ras et al. [7]. Solid and dashed lines are overlapped. DMM3: OME₃.

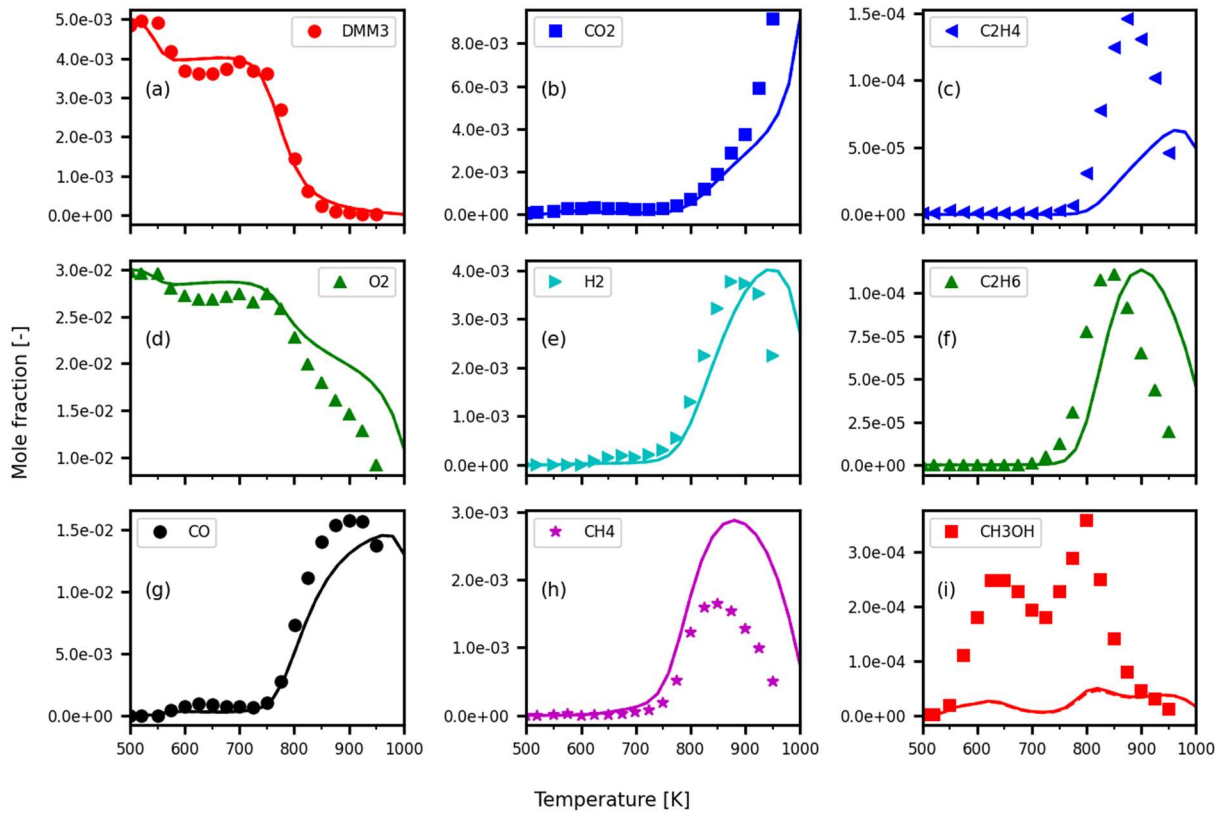


Figure S 23: Oxidation of $\text{OME}_3/\text{O}_2/\text{N}_2$ in a jet-stirred reactor at $\phi = 1.0$, 1 atm and $\tau = 2$ s. Symbols: experimental data from Qiu et al. [15], solid lines: this model, dashed lines: implementing $\text{OME}_3 + \text{CH}_3\text{O}$ reaction rate from Ras et al. [7]. Solid and dashed lines are overlapped. DMM3: OME_3 .

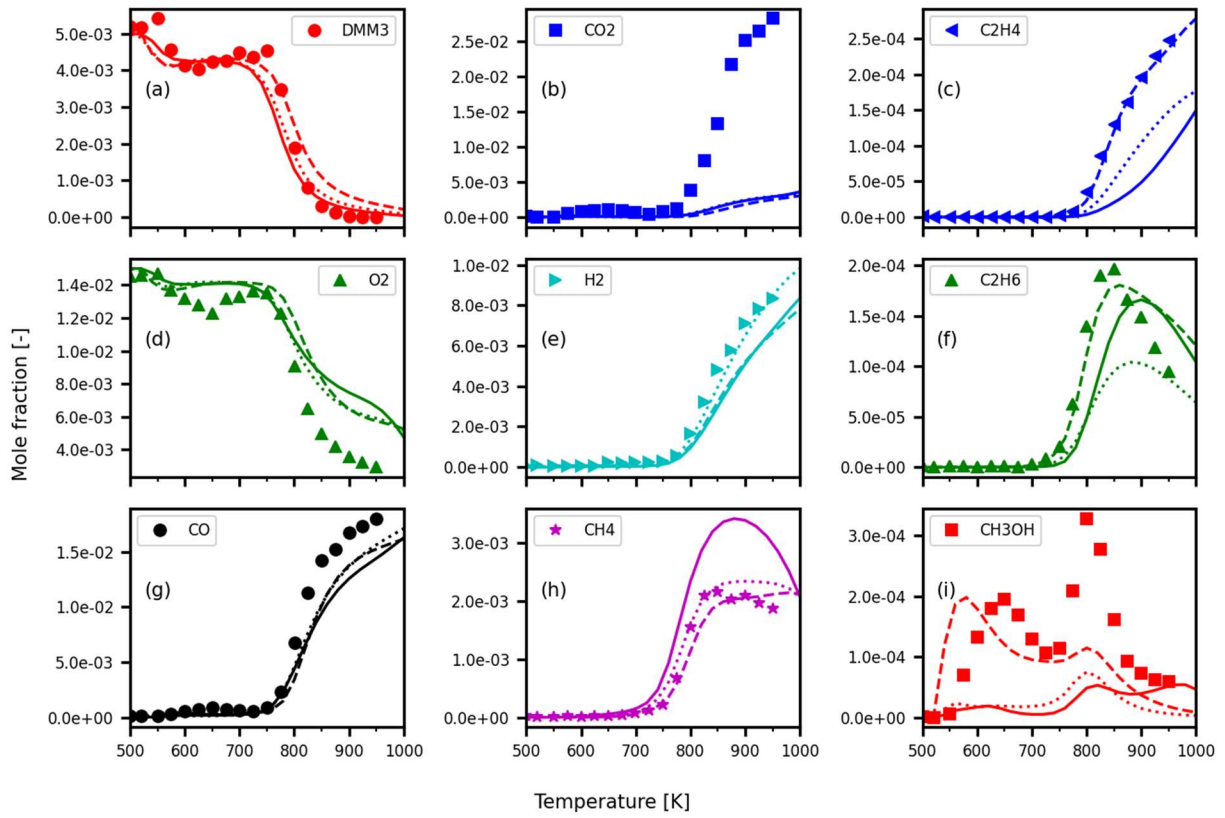


Figure S 24: Oxidation of $\text{OME}_3/\text{O}_2/\text{N}_2$ in a jet-stirred reactor at $\phi = 2.0$, 1 atm and $\tau = 2$ s. Symbols: experimental data from Qiu et al. [15], solid lines: this model, dashed lines: Cai model [5], dotted lines: He model [1]. DMM3: OME_3 .

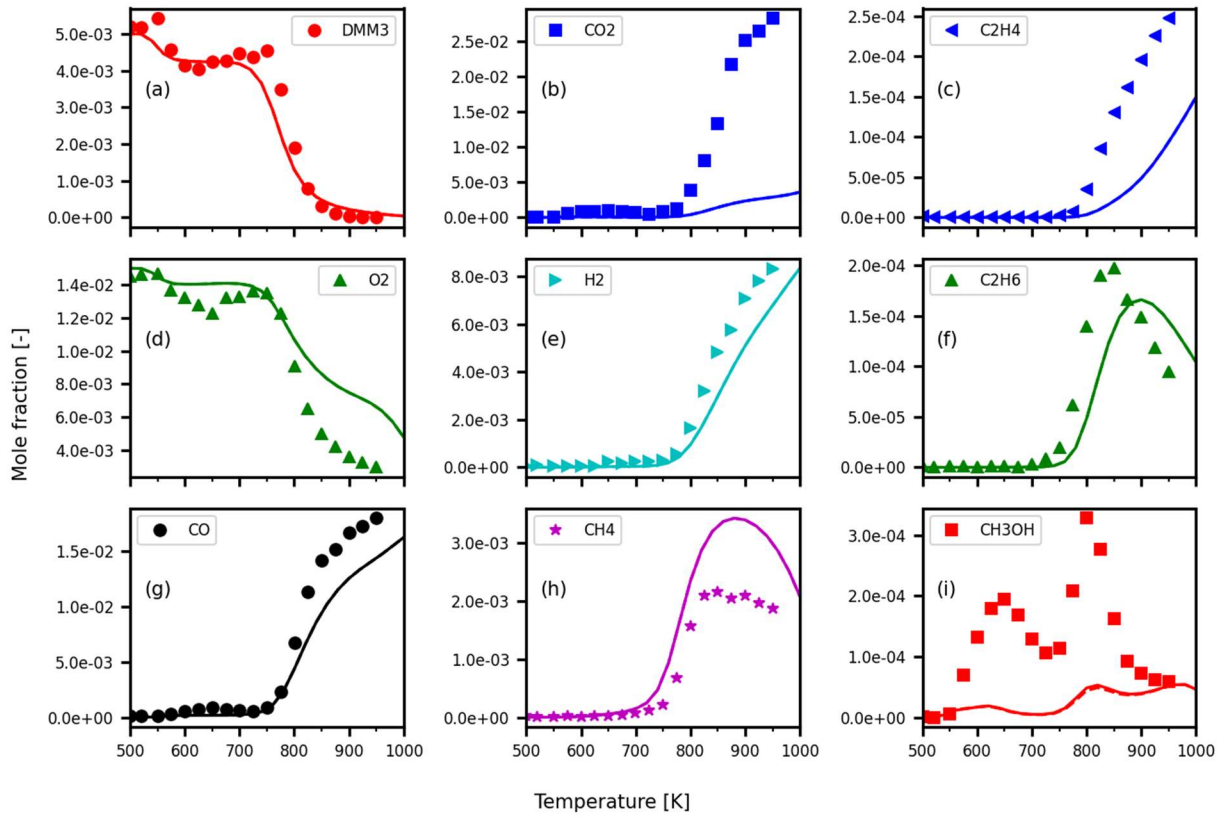


Figure S 25: Oxidation of $\text{OME}_3/\text{O}_2/\text{N}_2$ in a jet-stirred reactor at $\phi = 2.0$, 1 atm and $\tau = 2$ s. Symbols: experimental data from Qiu et al. [15], solid lines: this model, dashed lines: implementing $\text{OME}_3 + \text{CH}_3\text{O}$ reaction rate from Ras et al. [7]. Solid and dashed lines are overlapped. DMM3: OME_3 .

5. Speciation in a flow reactor - OME₂, and OME₃

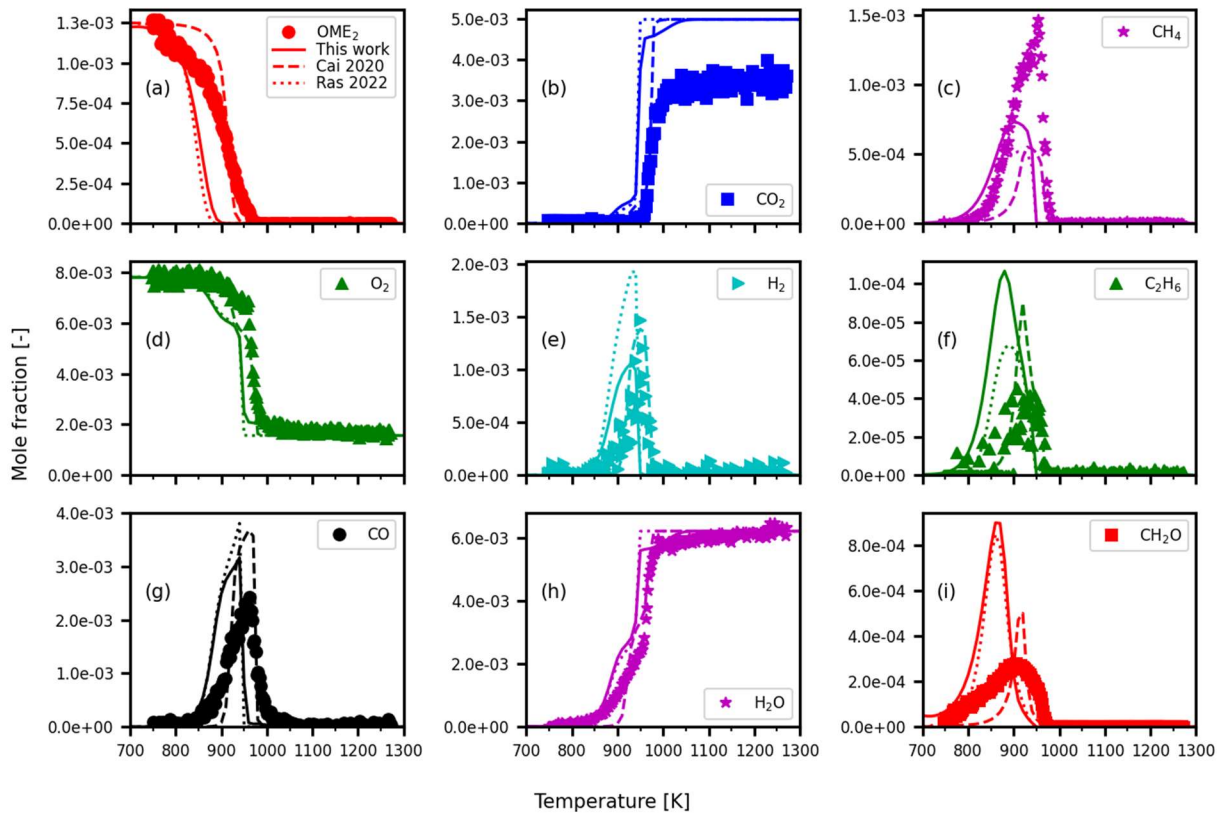


Figure S 26: Oxidation of OME₂/O₂/Ar in a flow reactor at $\phi = 0.8$, 1 atm and $\tau = 1.7 - 2.8$ s. Symbols: experimental data from Gaiser et al. [16], solid lines: this model, dashed lines: Cai model [5], dotted lines: Ras model [7].

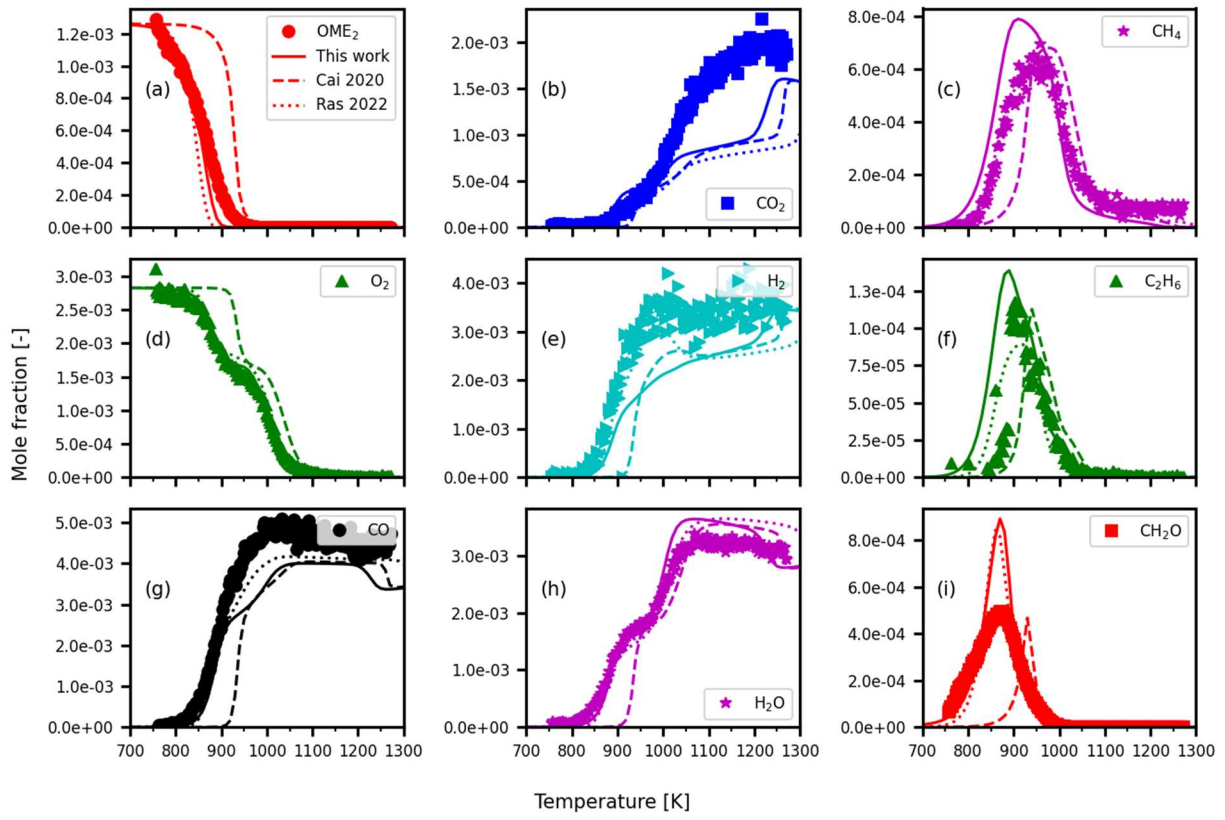


Figure S 27: Oxidation of OME₂/O₂/Ar in a flow reactor at $\phi = 2.0$, 1 atm and $\tau = 1.7 - 2.8$ s. Symbols experimental data from Gaiser et al. [16], solid lines: this model, dashed lines: Cai model [5], dotted lines: Ras model [7].

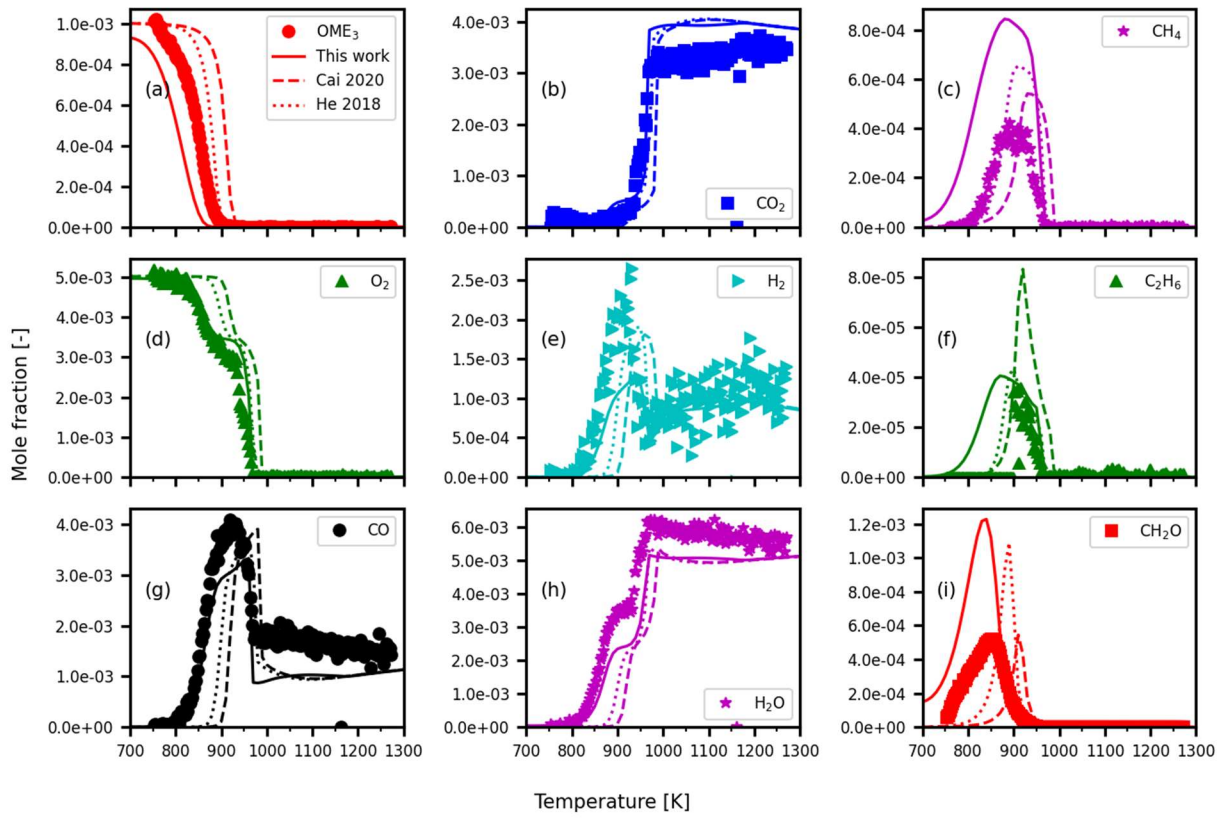


Figure S 28: Oxidation of $\text{OME}_3/\text{O}_2/\text{Ar}$ in a flow reactor at $\phi = 1.2$, 1 atm and $\tau = 1.7 - 2.8$ s. Symbols: experimental data from Gaiser et al. [16], solid lines: this model, dashed lines: Cai model [5], dotted lines: He model [1].

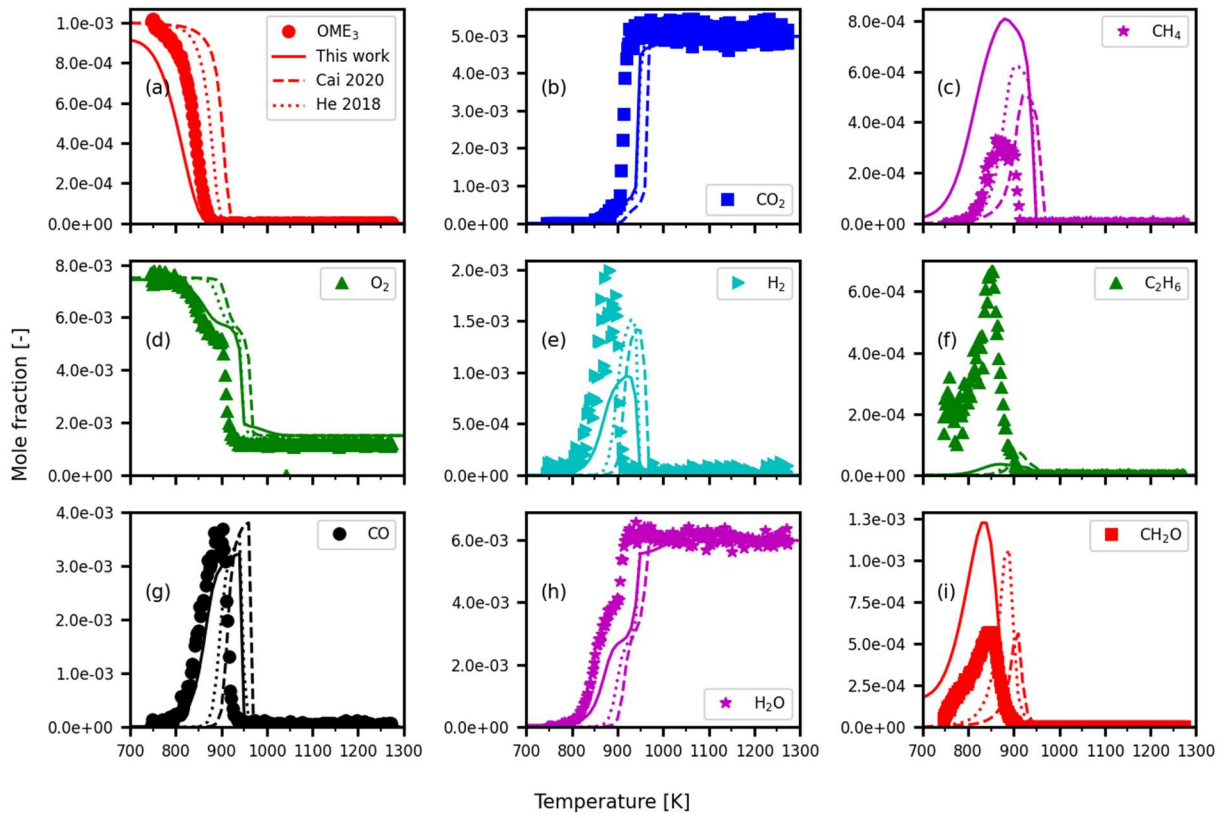


Figure S 29: Oxidation of $\text{OME}_3/\text{O}_2/\text{Ar}$ in a flow reactor at $\phi = 0.8$, 1 atm and $\tau = 1.7 - 2.8$ s. Symbols experimental data from Gaiser et al. [16] [15], solid lines: this model, dashed lines: Cai model [5], dotted lines: He model [1].

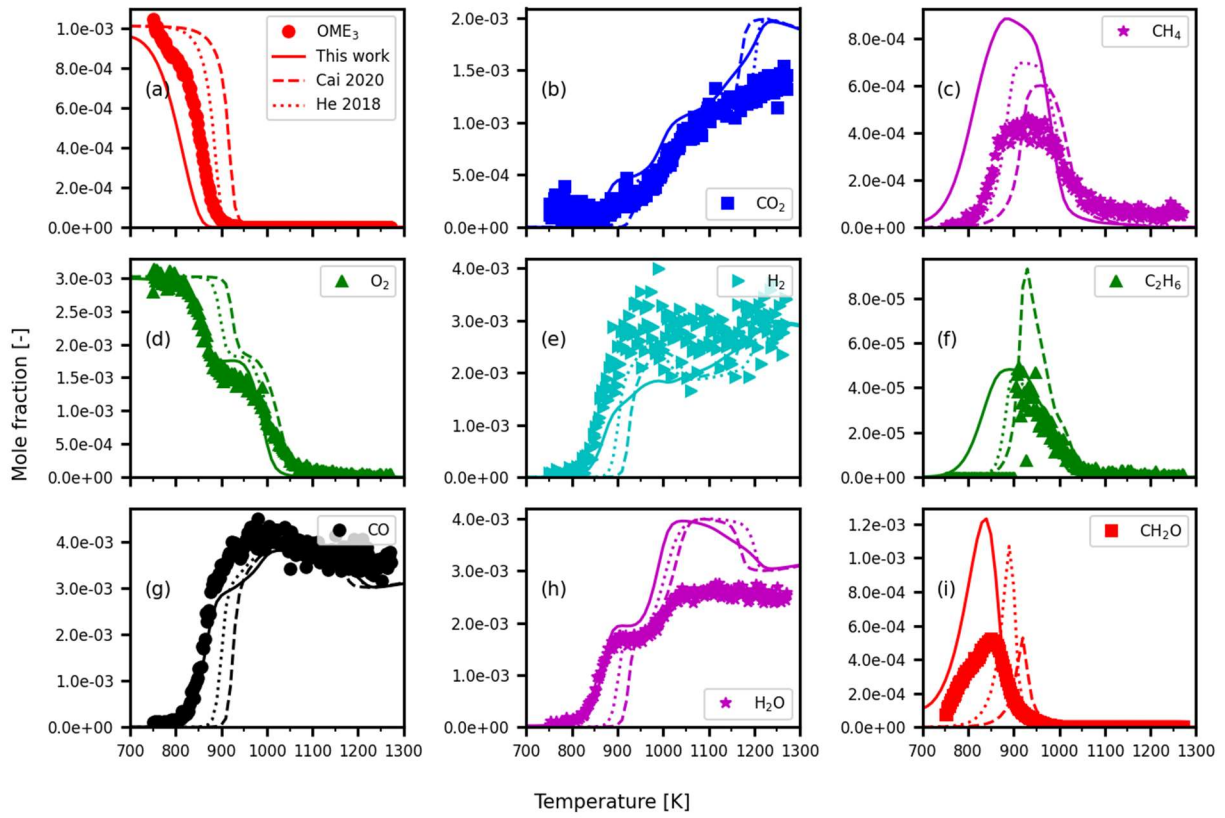


Figure S 30: Oxidation of OME₃/O₂/Ar in a flow reactor at $\phi = 2.0$, 1 atm and $\tau = 1.7 - 2.8$ s. Symbols experimental data from Gaiser et al. [16], solid lines: this model, dashed lines: Cai model [5], dotted lines: He model [1].

6. Speciation in burner stabilized flame – OME₂ and OME₃

Figures S31 - S33 show the speciation history in low-pressure burner stabilized flame fueled by OME₂/O₂/Ar and OME₃/O₂/Ar at rich ($\phi = 1.7$) and stoichiometric conditions, respectively. Simulations were conducted imposing the experimental temperature profile. As seen, the proposed model satisfactorily predicts the evolution of various species. We further demonstrate the robustness of our comprehensive kinetic model by validating extensively against a wide range of experimental data.

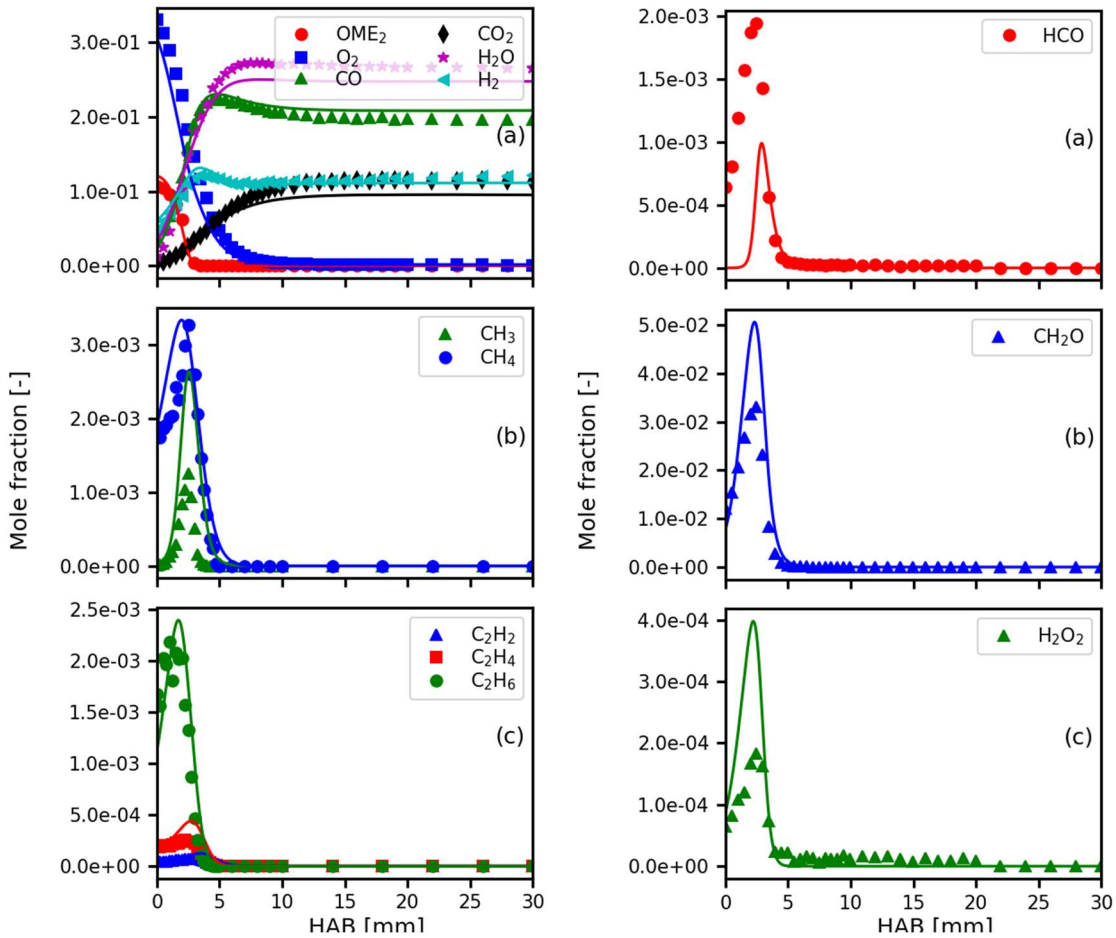


Figure S 31: Speciation of OME₂/O₂/Ar oxidation in a burner stabilized flame at $\phi = 1.7$, $P_u = 4$ kPa, and $T_u = 333$ K. Symbols: experiments from Gaiser et al. [16], lines: model predictions from this work imposing experimental temperature profile.

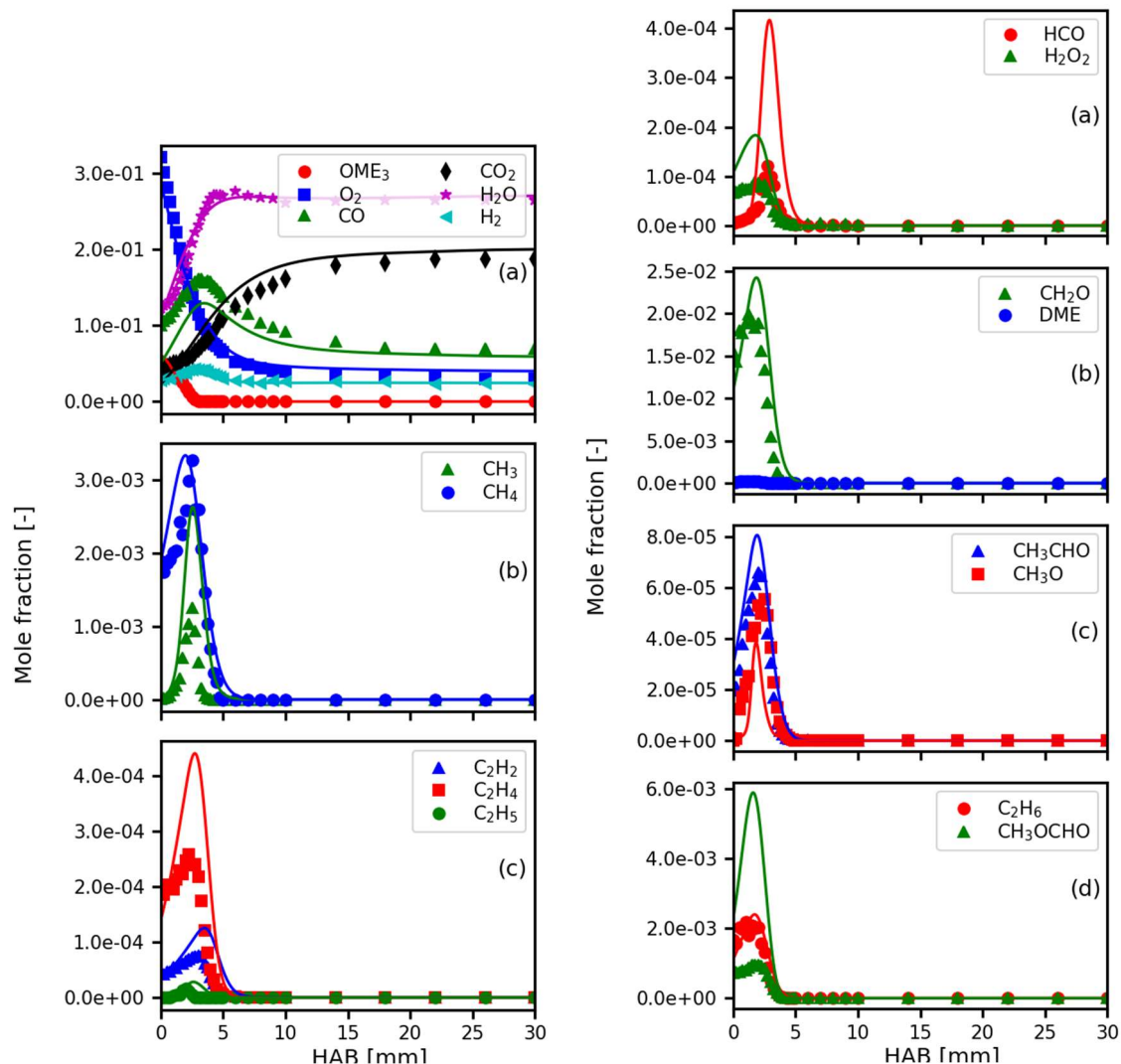


Figure S 32: Speciation of $\text{OME}_3/\text{O}_2/\text{Ar}$ oxidation in a burner stabilized flame at $\phi = 1.0$, $P_u = 3.33 \text{ kPa}$, and $T_u = 298 \text{ K}$. Symbols: experiments from Sun et al. [10], lines: model predictions from this work imposing experimental temperature profile.

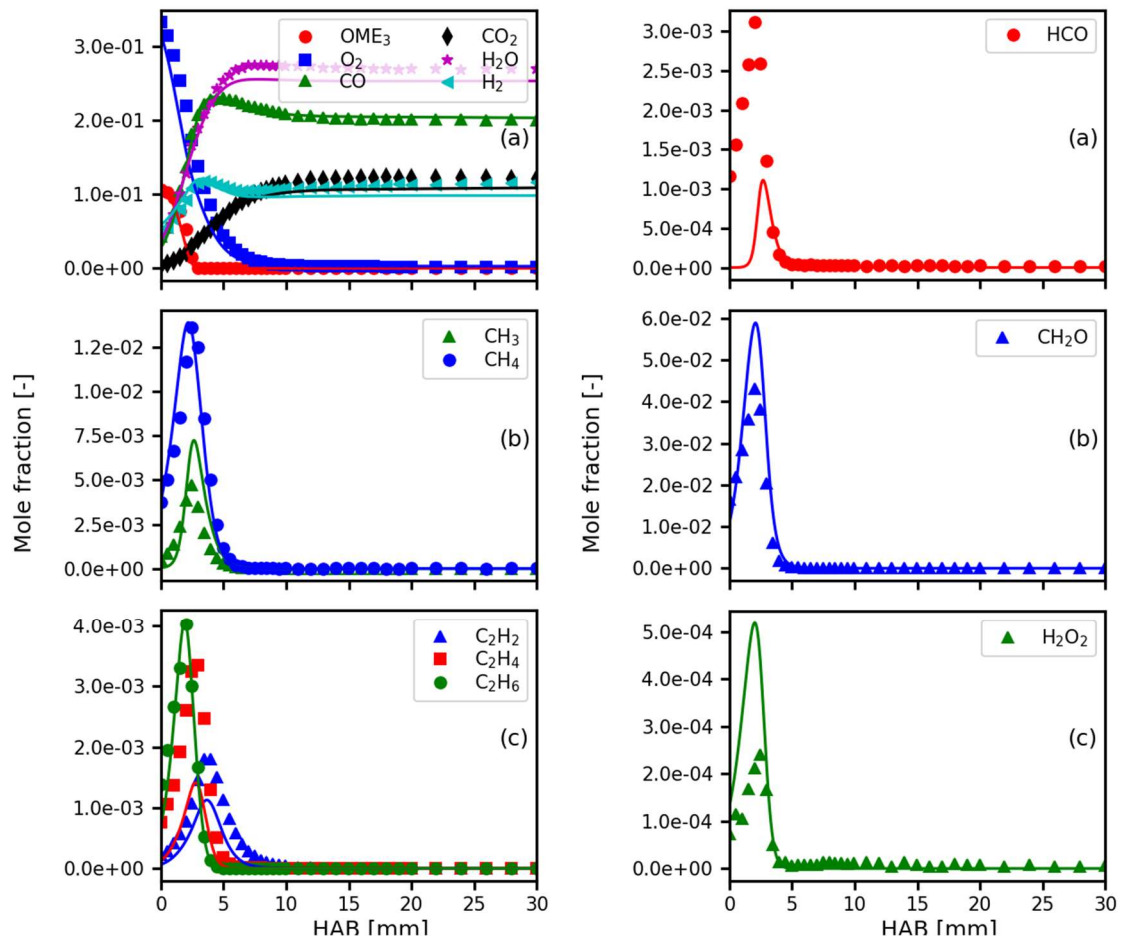


Figure S 33: Speciation of OME₃/O₂/Ar oxidation in a burner stabilized flame at $\phi = 1.7$, 4 kPa, and 333 K. Symbols: experiments from Gaiser et al. [16], lines: model predictions from this work imposing experimental temperature profile.

7. OME₀ (DME) - Validation

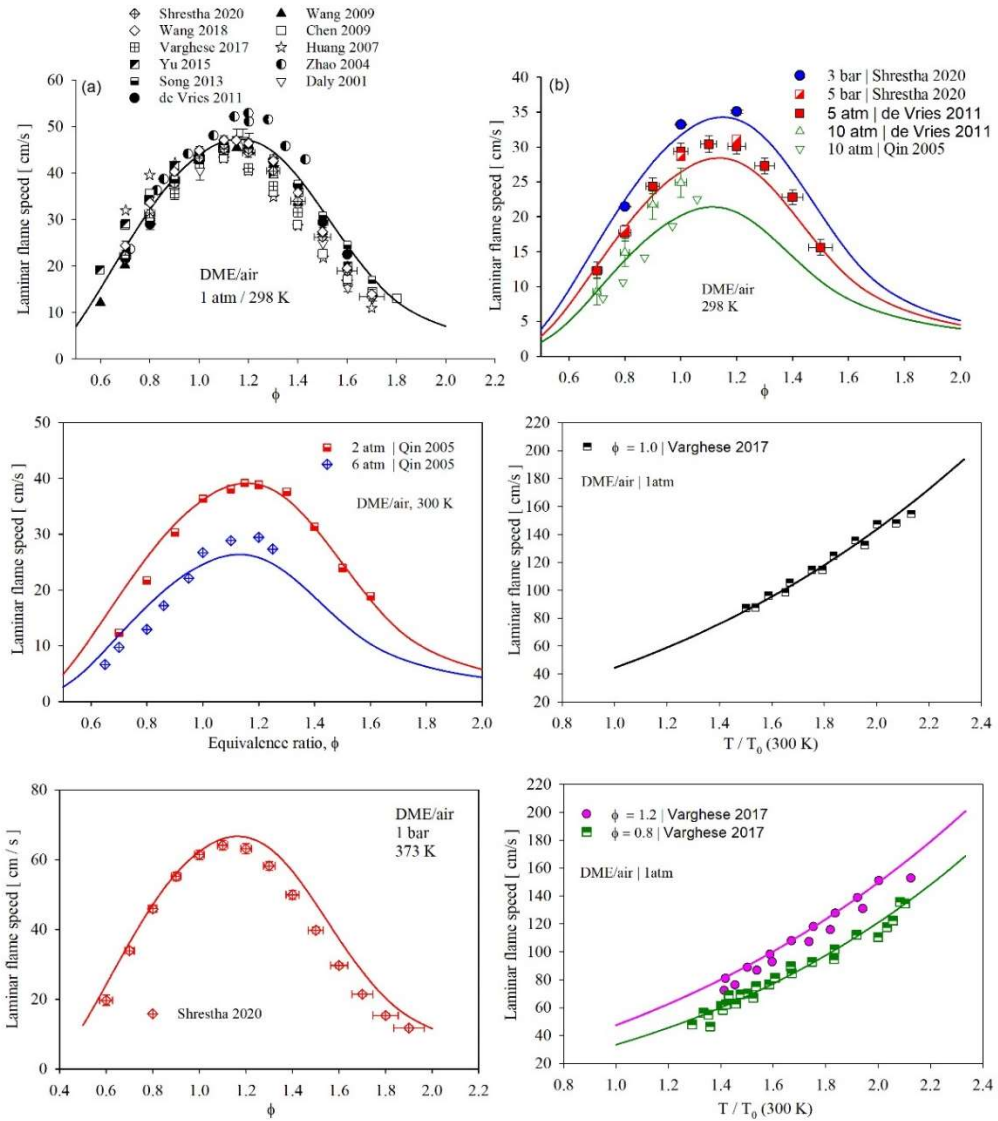


Figure S 34: Laminar flame speed of DME/air at different conditions. Lines: model predictions from this work. Symbols: experimental data from literature [4,17–26].

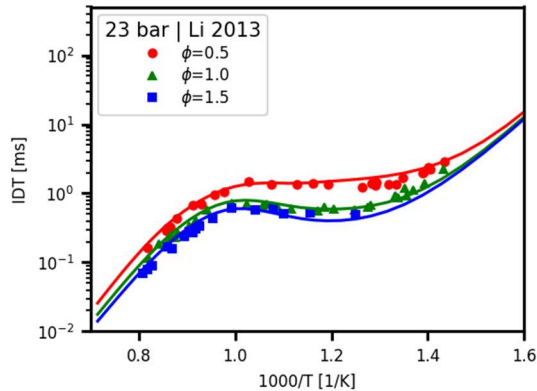


Figure S 35: Ignition delay time of DME/air at 23 bar and different equivalence ratio. Symbols: experiments [27], lines: model predictions from this work.

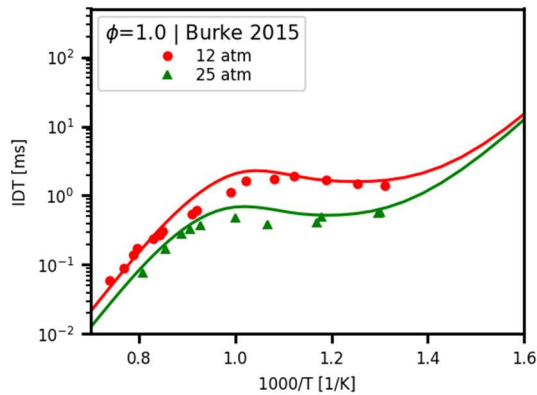


Figure S 36: Ignition delay time of DME/air at $\phi = 1.0$ bar and different pressure. Symbols: experiments [28], lines: model predictions from this work.

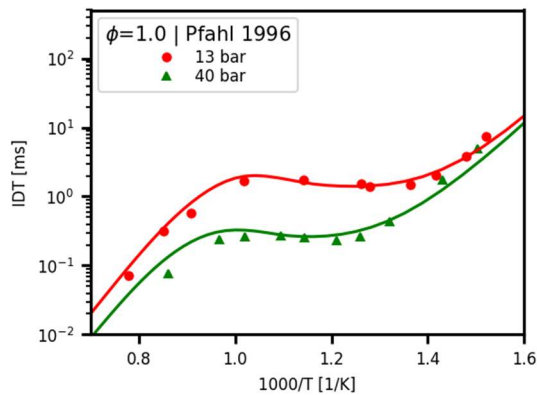


Figure S 37: Ignition delay time of DME/air at $\phi = 1.0$ bar and different pressure. Symbols: experiments [29], lines: model predictions from this work.

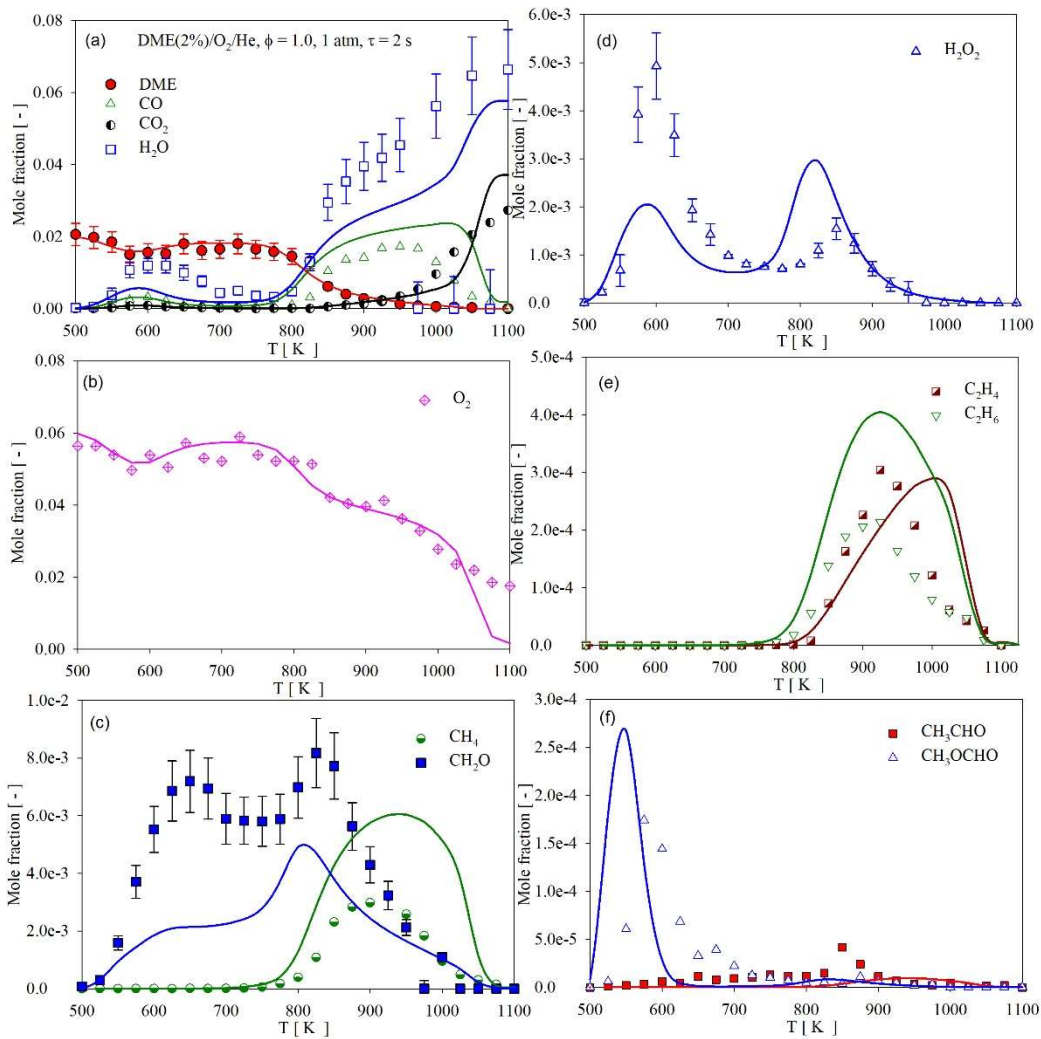


Figure S 38: DME/O₂/He oxidation in a jet-stirred reactor at $\phi = 1.0$, 1 atm and $\tau = 2.0$ s. Symbols: experimental data from Rodriguez et al. [30], lines: model predictions from this work.

References

- [1] T. He, Z. Wang, X. You, H. Liu, Y. Wang, X. Li, X. He, A chemical kinetic mechanism for the low- and intermediate-temperature combustion of Polyoxymethylene Dimethyl Ether 3 (PODE3), *Fuel.* 212 (2018) 223–235. doi:10.1016/j.fuel.2017.09.080.
- [2] X. Zhong, H. Wang, Q. Zuo, Z. Zheng, J. Wang, W. Yin, M. Yao, Experimental and kinetic modeling studies of polyoxymethylene dimethyl ether (PODE) pyrolysis in jet stirred reactor, *J. Anal. Appl. Pyrolysis.* 159 (2021) 105332. doi:10.1016/j.jaat.2021.105332.
- [3] C. Zhang, J. He, Y. Li, X. Li, P. Li, Ignition delay times and chemical kinetics of diethoxymethane/O₂/Ar mixtures, *Fuel.* 154 (2015) 346–351. doi:10.1016/j.fuel.2015.04.005.
- [4] K.P. Shrestha, S. Eckart, A.M. Elbaz, B.R. Giri, C. Fritzsche, L. Seidel, W.L. Roberts, H. Krause, F. Mauss, A comprehensive kinetic model for dimethyl ether and dimethoxymethane oxidation and NO_x interaction utilizing experimental laminar flame speed measurements at elevated pressure and temperature, *Combust. Flame.* 218 (2020) 57–74. doi:10.1016/j.combustflame.2020.04.016.
- [5] L. Cai, S. Jacobs, R. Langer, F. vom Lehn, K.A. Heufer, H. Pitsch, Auto-ignition of oxymethylene ethers (OMEn, n = 2–4) as promising synthetic e-fuels from renewable electricity: shock tube experiments and automatic mechanism generation, *Fuel.* 264 (2020) 116711. doi:10.1016/J.FUEL.2019.116711.
- [6] W. Ludwig, B. Brandt, G. Friedrichs, F. Temps, Kinetics of the reaction C₂H₅ + HO₂ by time-resolved mass spectrometry, *J. Phys. Chem. A.* 110 (2006) 3330–3337. doi:10.1021/jp0557464.
- [7] K. De Ras, M. Kusenberg, G. Vanhove, Y. Fenard, A. Eschenbacher, R.J. Varghese, J. Aerssens, R. Van de Vijver, L.-S. Tran, J.W. Thybaut, K.M. Van Geem, A detailed experimental and kinetic modeling study on pyrolysis and oxidation of oxymethylene ether-2 (OME-2), *Combust. Flame.* 238 (2022) 111914. doi:10.1016/J.COMBUSTFLAME.2021.111914.
- [8] S. Eckart, L. Cai, C. Fritzsche, F. vom Lehn, H. Pitsch, H. Krause, Laminar burning velocities, CO, and NO_x emissions of premixed polyoxymethylene dimethyl ether flames, *Fuel.* 293 (2021) 120321. doi:10.1016/j.fuel.2021.120321.
- [9] Q. Wang, W. Sun, L. Guo, S. Lin, P. Cheng, H. Zhang, Y. Yan, Experimental and kinetic study on the laminar burning speed, Markstein length and cellular instability of oxygenated fuels, *Fuel.* 297 (2021) 120754. doi:10.1016/j.fuel.2021.120754.
- [10] W. Sun, G. Wang, S. Li, R. Zhang, B. Yang, J. Yang, Y. Li, C.K. Westbrook, C.K. Law, Speciation and the laminar burning velocities of poly(oxymethylene) dimethyl ether 3 (POMDME3) flames: An experimental and modeling study, *Proc. Combust. Inst.* 36 (2017) 1269–1278. doi:10.1016/j.proci.2016.05.058.

- [11] J.M. Ngugi, S. Richter, M. Braun-Unkhoff, C. Naumann, M. Köhler, U. Riedel, A Study on Fundamental Combustion Properties of Oxymethylene Ether-2, *J. Eng. Gas Turbines Power.* 144 (2022) 011014–1. doi:10.1115/1.4052097.
- [12] S. Drost, R. Schießl, M. Werler, J. Sommerer, U. Maas, Ignition delay times of polyoxymethylene dimethyl ether fuels (OME2 and OME3) and air: Measurements in a rapid compression machine, *Fuel.* 258 (2019) 116070. doi:10.1016/j.fuel.2019.116070.
- [13] F.R. Gillespie, An experimental and modelling study of the combustion of oxygenated hydrocarbons, National University of Ireland, 2014. doi:10.1039/b809078p.
- [14] W. Sun, T. Tao, M. Lailliau, N. Hansen, B. Yang, P. Dagaut, Exploration of the oxidation chemistry of dimethoxymethane: Jet-stirred reactor experiments and kinetic modeling, *Combust. Flame.* 193 (2018) 491–501. doi:10.1016/j.combustflame.2018.04.008.
- [15] Z. Qiu, A. Zhong, Z. Huang, D. Han, An experimental and modeling study on polyoxymethylene dimethyl ether 3 (PODE3) oxidation in a jet stirred reactor, *Fundam. Res.* (2021). doi:10.1016/j.fmre.2021.09.005.
- [16] N. Gaiser, T. Bierkandt, P. Oßwald, J. Zinsmeister, T. Kathrotia, S. Shaqiri, P. Hemberger, T. Kasper, M. Aigner, M. Köhler, Oxidation of oxymethylene ether (OME0–5): An experimental systematic study by mass spectrometry and photoelectron photoion coincidence spectroscopy, *Fuel.* 313 (2022) 122650. doi:10.1016/j.fuel.2021.122650.
- [17] R.J. Varghese, V.R. Kishore, M. Akram, Y. Yoon, S. Kumar, Burning velocities of DME(dimethyl ether)-air premixed flames at elevated temperatures, *Energy.* 126 (2017) 34–41. doi:10.1016/j.energy.2017.03.004.
- [18] Z. Chen, L. Wei, Z. Huang, H. Miao, X. Wang, Measurement of Laminar Burning Velocities of Dimethyl Ether - Air Premixed Mixtures with N₂ and CO₂ Dilution, 86 (2009) 735–739.
- [19] W.S. Song, S.W. Jung, J. Park, O.B. Kwon, Y.J. Kim, T.H. Kim, J.H. Yun, S.I. Keel, Effects of syngas addition on flame propagation and stability in outwardly propagating spherical dimethyl ether-air premixed flames, *Int. J. Hydrogen Energy.* 38 (2013) 14102–14114. doi:10.1016/j.ijhydene.2013.08.037.
- [20] J. de Vries, W.B. Lowry, Z. Serinyel, H.J. Curran, E.L. Petersen, Laminar flame speed measurements of dimethyl ether in air at pressures up to 10 atm, *Fuel.* 90 (2011) 331–338. doi:10.1016/j.fuel.2010.07.040.
- [21] Y.L. Wang, A.T. Holley, C. Ji, F.N. Egolfopoulos, T.T. Tsotsis, H.J. Curran, Propagation and extinction of premixed dimethyl-ether/air flames, *Proc. Combust. Inst.* 32 I (2009) 1035–1042. doi:10.1016/j.proci.2008.06.054.
- [22] H. Yu, E. Hu, Y. Cheng, K. Yang, X. Zhang, Z. Huang, Effects of hydrogen addition on the laminar flame speed and markstein length of premixed dimethyl ether-air flames, *Energy and Fuels.* 29 (2015) 4567–4575. doi:10.1021/acs.energyfuels.5b00501.
- [23] X. Qin, Y. Ju, Measurements of burning velocities of dimethyl ether and air premixed flames at elevated pressures, *Proc. Combust. Inst.* 30 (2005) 233–240.

doi:10.1016/j.proci.2004.08.251.

- [24] C.A. Daly, J.M. Simmie, J. Würmel, N. Djeballi, C. Paillard, Burning velocities of dimethyl ether and air, *Combust. Flame*. 125 (2001) 1329–1340. doi:10.1016/S0010-2180(01)00249-8.
- [25] Z. Zhao, A. Kazakov, F.L. Dryer, Measurements of dimethyl ether/air mixture burning velocities by using particle image velocimetry, *Combust. Flame*. 139 (2004) 52–60. doi:10.1016/j.combustflame.2004.06.009.
- [26] Z. Huang, Q. Wang, J. Yu, Y. Zhang, K. Zeng, H. Miao, D. Jiang, Measurement of laminar burning velocity of dimethyl ether-air premixed mixtures, *Fuel*. 86 (2007) 2360–2366. doi:10.1016/j.fuel.2007.01.021.
- [27] Z. Li, W. Wang, Z. Huang, M.A. Oehlschlaeger, Dimethyl ether autoignition at engine-relevant conditions, *Energy and Fuels*. 27 (2013) 2811–2817. doi:10.1021/ef400293z.
- [28] U. Burke, K.P. Somers, P. O'Toole, C.M. Zinner, N. Marquet, G. Bourque, E.L. Petersen, W.K. Metcalfe, Z. Serinyel, H.J. Curran, An ignition delay and kinetic modeling study of methane, dimethyl ether, and their mixtures at high pressures, *Combust. Flame*. 162 (2015) 315–330. doi:10.1016/j.combustflame.2014.08.014.
- [29] U. Pfahl, K. Fieweger, G. Adomeit, Self-ignition of diesel-relevant hydrocarbon-air mixtures under engine conditions, *Symp. Combust.* 26 (1996) 781–789.
- [30] A. Rodriguez, O. Frottier, O. Herbinet, R. Fournet, R. Bounaceur, C. Fittschen, F. Battin-Leclerc, Experimental and Modeling Investigation of the Low-Temperature Oxidation of Dimethyl Ether, *J. Phys. Chem. A*. 119 (2015) 7905–7923. doi:10.1021/acs.jpca.5b01939.